Late Cretaceous–Neogene trends in deep ocean temperature and continental ice volume: Reconciling records of benthic foraminiferal geochemistry ($\delta^{18}O$ and Mg/Ca) with sea level history

B. S. Cramer,[1] K. G. Miller,[2] P. J. Barrett,[3] and J. D. Wright[2]

Received 29 April 2011; revised 28 September 2011; accepted 3 October 2011; published 16 December 2011.

[1] We reconstruct trends in ice volume and deep ocean temperature for the past 108 Myr, resolving variations on timescales of ~2 Myr and longer. We use a sea level record as a proxy for ice volume, a benthic foraminiferal Mg/Ca_{bf} record as a proxy for temperature, and a benthic foraminiferal $\delta^{18}O_{bf}$ record as a proxy for both. This allows us to construct dual estimates of temperature and ice volume variations for the interval 10–60 Ma: extracting temperature from $\delta^{18}O_{bf}$ by using sea level as a proxy for ice volume to constrain the $\delta^{18}O_{sw}$ component, and extracting seawater $\delta^{18}O_{sw}$ (which reflects ice volume) from $\delta^{18}O_{bf}$ by using Mg/Ca_{bf} to constrain the temperature component. Each of these approaches requires numerous assumptions, but the range of plausible solutions are concordant on timescales >2 Myr and within an uncertainty of ±2°C temperature and ±0.4‰ $\delta^{18}O_{sw}$. The agreement between the two approaches for the last 50 Myr provides empirical justification for the use of $\delta^{18}O_{bf}$, Mg/Ca_{bf}, and sea level records as robust climate proxies. Our reconstructions indicate differences between deep ocean cooling and continental ice growth in the late Cenozoic: cooling occurred gradually in the middle–late Eocene and late Miocene–Pliocene while ice growth occurred rapidly in the earliest Oligocene, middle Miocene, and Plio-Pleistocene. These differences are consistent with climate models that imply that temperatures, set by the long-term CO_2 equilibrium, should change only gradually on timescales >2 Myr, but growth of continental ice sheets may be rapid in response to climate thresholds due to feedbacks that are not yet fully understood.

Citation: Cramer, B. S., K. G. Miller, P. J. Barrett, and J. D. Wright (2011), Late Cretaceous–Neogene trends in deep ocean temperature and continental ice volume: Reconciling records of benthic foraminiferal geochemistry ($\delta^{18}O$ and Mg/Ca) with sea level history, *J. Geophys. Res.*, *116*, C12023, doi:10.1029/2011JC007255.

1. Introduction

[2] Trends drawn through compilations of benthic foraminiferal oxygen isotope measurements ($\delta^{18}O_{bf}$; see notation section at end of text for a glossary of abbreviated terminology) have long been used as a primary proxy for Cenozoic climate variations [*Emiliani*, 1954, 1961; *Savin et al.*, 1975; *Savin*, 1977; *Shackleton and Kennett*, 1975; *Miller et al.*, 1987; *Zachos et al.*, 2001, 2008; *Cramer et al.*, 2009]. These trends are robust estimators of variability on >1 Myr timescales, although they do not resolve the persistent orbitally driven climate cyclicity at <1 Myr timescales that is present in individual high resolution records. The $\delta^{18}O_{bf}$ trend is recognized as a proxy for a combination of two climate parameters: deep ocean temperatures that are presumed to reflect surface temperatures at high latitudes where most deep waters are formed, and the seawater $\delta^{18}O$ value ($\delta^{18}O_{sw}$) that reflects global ice volume (local evaporation/precipitation differences that affect surface water $\delta^{18}O_{sw}$ are damped in the deep sea). The interpretation of climate variations from $\delta^{18}O_{bf}$ trends is therefore ambiguous as to the separate variations in high latitude temperature and ice volume, especially during the late Paleogene–Neogene interval that is characterized by large variations in ice volume. Taking modern deep ocean temperatures as a minimal constraint on deep ocean temperatures in an ice-free world, *Miller et al.* [1987] used the $\delta^{18}O_{bf}$ record to demonstrate the existence of large ice sheets since the earliest Oligocene. This was later confirmed by the finding of ice-rafted and grounded-ice debris in drill cores from the Antarctic continental shelf [*Barrett*, 1989; *Hambrey et al.*, 1991] and from ice rafted material in the Southern Ocean [*Zachos et al.*, 1992]. While it seems reasonable to assume that high latitude surface temperatures and global ice volume covary on long timescales [e.g., *Crowley and Kim*, 1995; *Zachos et al.*, 2001; *Hansen et al.*, 2008], that assumption is at odds with models indicating a nonlinear response of ice volume to temperature [e.g., *DeConto and Pollard*, 2003].

[1]Theiss Research, Eugene, Oregon, USA.
[2]Department of Earth and Planetary Sciences, Rutgers, State University of New Jersey, Piscataway, New Jersey, USA.
[3]Antarctic Research Centre, Victoria University, Wellington, New Zealand.

0148-0227/11/2011JC007255

[3] An independent constraint on ice volume or deep ocean temperature is necessary to separate the ice volume and temperature components of the $\delta^{18}O_{bf}$ record. One approach has been to use the Mg/Ca ratio in benthic foraminiferal tests (Mg/Ca_{bf}) as an independent proxy for deep ocean temperature [*Lear et al.*, 2000, 2003, 2004; *Billups and Schrag*, 2002, 2003; *Dutton et al.*, 2004; *Shevenell et al.*, 2008; *Sosdian and Rosenthal*, 2009; *Billups and Scheiderich*, 2010; *Dawber and Tripati*, 2011]. Over long timescales (10–100 Myr), this method suffers from a lack of sufficient constraint on the seawater Mg/Ca ratio (Mg/Ca_{sw}), which creates a large uncertainty in the temperature contribution to $\delta^{18}O_{bf}$ [*Billups and Schrag*, 2002, 2003]. On short timescales (<1 Myr), the combination of deep ocean Mg/Ca_{bf} and $\delta^{18}O_{bf}$ implies unexpectedly small temperature changes and large ice volumes, most notably in earliest Oligocene records where deep ocean Mg/Ca_{bf} records imply a warming interval lasting ~2 Myr [*Lear et al.*, 2000, 2004; *Billups and Schrag*, 2003] that is at odds with evidence for high latitude surface cooling [*Liu et al.*, 2009; *Eldrett et al.*, 2009] as well as cooling implied by Mg/Ca_{bf} records from shallow water sections [*Lear et al.*, 2008; *Katz et al.*, 2008]. This has highlighted the effect of the seawater carbonate ion saturation state ($\Delta[CO_3^{=}]$) on Mg/Ca_{bf}: an increase in $\Delta[CO_3^{=}]$ as reflected in the abrupt deepening of the CCD could explain the apparent warming in deep ocean Mg/Ca_{bf} records coincident with glaciation of Antarctica in the earliest Oligocene [*Lear et al.*, 2000, 2004, 2008, 2010; *Billups and Schrag*, 2003; *Coxall et al.*, 2005; *Katz et al.*, 2008; *Peck et al.*, 2010; *Pusz et al.*, 2011]. Recent studies using core top benthic foraminifera have demonstrated a clear correlation between Mg/Ca_{bf} and $\Delta[CO_3^{=}]$, but it has not been definitively shown that this effect is important at high temperatures (≫5°C) or high $\Delta[CO_3^{=}]$ (>25 μmol/kg) [*Elderfield et al.*, 2006; *Yu and Elderfield*, 2008; *Healey et al.*, 2008; *Bryan and Marchitto*, 2008; *Raitzsch et al.*, 2008].

[4] Sequence stratigraphic records have been used to reconstruct sea level changes and confirm that specific $\delta^{18}O_{bf}$ increases in the Cenozoic and Late Cretaceous correspond with rapid (≪1 Myr) sea level falls caused by ice volume increases [*Browning et al.*, 1996; *Pekar and Miller*, 1996; *Miller et al.*, 1996, 1999, 2005, 2011]. On Myr timescales, sea level reconstructions generally provide only a minimum estimate of ice-volume changes because sea level lowstands are typically not recorded [e.g., *Miller et al.*, 2005]. On 10–100 Myr timescales, sea level may also be affected by variations in the volume of the ocean basins due to changes in globally integrated seafloor spreading rates [e.g., *Cogné et al.*, 2006; *Müller et al.*, 2008; *Rowley*, 2002, 2008]. While the amplitudes of individual sea level falls have been compared with $\delta^{18}O_{bf}$ increases, the sea level record has not previously been used to constrain the ice volume component of a $\delta^{18}O_{bf}$ record prior to the Plio-Pleistocene.

[5] Because of the number of different assumptions that must be made in order to calculate temperature from Mg/Ca_{sw} or $\delta^{18}O_{sw}$ from sea level (in order to subtract from $\delta^{18}O_{bf}$) the uncertainty associated with using either of these approaches on its own is large (±10–15 m or ± 4°C) (K. G. Miller et al., The high tide of the warm Pliocene: Implications of global sea level for Antarctic deglaciation, submitted to *Geology*, 2011). However, we demonstrate that combining these three proxies (Mg/Ca_{bf}, $\delta^{18}O_{bf}$ and sea level) subject to the constraint of ice-free conditions in the early Eocene produces credible dual records of deep ocean temperature and ice volume variations since 50 Ma.

[6] In the next section of this paper we describe in detail the available constraints on parameters and equations necessary for the interpretation of $\delta^{18}O_{bf}$ (section 2.1), Mg/Ca_{bf} (section 2.2), and sea level (section 2.3) records. In section 3 we examine the results of calculations using the three proxy records, and the implications for parameters and equations that are poorly constrained. We give particular attention to the implications of the Cenozoic Mg/Ca_{bf} record for constraining the dependence of Mg/Ca_{bf} on temperature, $\Delta[CO_3^{=}]$, and Mg/Ca_{sw}. In section 4 we discuss the potential implications of our results for understanding geologic processes and climate change through the Cenozoic. Reconstructions of variations in temperature and ice volume proxies (sea level, $\delta^{18}O_{sw}$) from our calculations are available in the auxiliary material.[1]

2. Primary Records: Characteristics and Limitations

[7] The primary records of the two geochemical proxies used in this study are analyses of sample series taken from ocean floor sediment cored by the Deep Sea Drilling Project, Ocean Drilling Program (http://odplegacy.org). These cores preserve records of climate change over millions of years at various locations in the ocean. The network of cores is not extensive enough to produce a complete oceanographic reconstruction for the Cenozoic; the records we use represent compilations of data representative of broad areas of the ocean. The paleo-water depth for each sample can be estimated using "backtracking" — applying an inverse model of tectonic subsidence to return the core location to its position at the time of deposition — and we use these estimates of paleo-water depth, calculated as described by *Cramer et al.* [2009], to control for water depth-dependent variations in the geochemical proxies.

[8] The age of individual core samples has typically been estimated by linear interpolation between bio- and magnetostratigraphic datums which in turn have been calibrated relative to radiometrically dated rock samples. The accuracy of this method is generally < ± 10% [see *Cande and Kent*, 1992], but the precision of correlation among cores using this method is much better: correlation of individual datums has a precision generally < ± 0.1 Myr and interpolation between datums does not add significantly to that uncertainty. Orbital stratigraphy allows correlation among sections at a precision <0.02 Myr, but orbital stratigraphies are not available for most of the records in our compilation. The correlation with the New Jersey sea level (NJSL) record has a significantly greater uncertainty of ±0.5 Myr [*Miller et al.*, 2005]. All records are shown relative to the GTS2004 timescale [*Gradstein et al.*, 2004] although most of the underlying data sets were originally published relative to the timescale of *Cande and Kent* [1992, 1995] or earlier timescales. Adjustment to the GTS2004 timescale was made by

[1] Auxiliary materials are available in the HTML. doi:10.1029/2011JC007255.

linear interpolation between ages of magnetic polarity chron boundaries given by *Ogg and Smith* [2004] and those in previous timescales.

[9] There is an inherent complication in combining time series that have been generated using different measurement techniques and pre-processed in different ways. The $\delta^{18}O_{bf}$ and Mg/Ca_{bf} trends used here were calculated using identical numerical techniques which should yield reconcilable records. However, we cannot rule out some artifactual differences especially at shorter wavelengths due to the higher sampling density of the underlying $\delta^{18}O_{bf}$ data set, the different processes that cause $\delta^{18}O_{bf}$ and Mg/Ca_{bf} to vary with temperature, and differing processes contributing to the noise in each measurement and reflected in the larger relative uncertainty associated with the Mg/Ca_{bf} trend estimate. The NJSL record is of substantially different character from the geochemical records: the record is not continuously sampled, having breaks at sequence boundaries so that sea level lowstand estimates are generally poorly constrained; as noted above, the precision of the underlying age models are generally not as good; and the numerical processing of the underlying data is completely different [see *Kominz et al.*, 2008]. We have attempted to compensate for the differences in numerical processing by smoothing the sea level record with a LOESS filter similar to that used to calculate the $\delta^{18}O_{bf}$ and Mg/Ca_{bf} trends, which should yield a record with a similar frequency response. The effect is a low-pass filter that passes >80% of the amplitude for frequencies <0.5 Myr^{-1} (wavelength >2 Myr) ramping down to <20% of the amplitude for frequencies >1.25 Myr^{-1} (wavelength <0.8 Myr) [see *Cramer et al.*, 2009].

2.1. $\delta^{18}O_{bf}$

[10] *Cramer et al.* [2009] compiled $\delta^{18}O_{bf}$ records and calculated separate trends for the North Atlantic (including equatorial), South Atlantic and subantarctic Southern, high latitude Southern, and tropical Pacific oceans extending through the Cenozoic and into the Late Cretaceous (0–80 Ma), with a less well-constrained trend based on two sites extending through the Late Cretaceous (to ~113 Ma). These records show that deep ocean $\delta^{18}O_{bf}$ was homogeneous among ocean basins during most of the Paleocene–Eocene (65–35 Ma), transitioning to heterogeneous deep ocean $\delta^{18}O_{bf}$ values in the Oligocene that reflect a thermal differentiation of northern and southern deepwater sources similar to the modern. On timescales greater than the mixing time of the ocean (~1 kyr), the growth and decay of ice affect the $\delta^{18}O$ of seawater on a global basis; variations in $\delta^{18}O_{bf}$ reflect these ice-driven changes as well as the mixing of water from temperature- and salinity-differentiated deep water source regions. Ice volume affects the global average $\delta^{18}O_{sw}$, so we should ideally use a global average of foraminiferal $\delta^{18}O$ measurements. Because the geographic and temporal distribution of data is too patchy for a meaningful global average $\delta^{18}O_{bf}$ value to be calculated, we use the Pacific record as the most representative monitor of deepwater conditions (black curve in Figure 1a). The Pacific basin has comprised the largest proportion of the global ocean volume throughout the Cenozoic, from ~60% today to >80% of the global reservoir in the Late Cretaceous–early Paleogene.

[11] The $\delta^{18}O_{bf}$ trends of *Cramer et al.* [2009] were calculated using $\delta^{18}O$ values measured on various species of benthic foraminifera corrected to the genus Cibicidoides (for the Neogene and Oligocene only analyses of Cibicidoides were used). It is common practice in the paleoceanographic literature, following *Shackleton* [1974], to assume that tests of the genus Uvigerina are precipitated at equilibrium with seawater and to use paleotemperature equations calibrated to $\delta^{18}O$ values for Uvigerina. More recently, it has become clear that the temperature-dependent oxygen isotopic fractionation between water and inorganic calcite determined by *Kim and O'Neil* [1997] is more consistent with $\delta^{18}O_{bf}$ values for Cibicidoides rather than Uvigerina (Figure 2a) [*Bemis et al.*, 1998; *Lynch-Stieglitz et al.*, 1999; *Costa et al.*, 2006; *Fontanier et al.*, 2006; *Bryan and Marchitto*, 2008]. Moreover, as noted by *Bemis et al.* [1998], the elevated pH in pore waters should be expected to affect the $\delta^{18}O$ values of the infaunal Uvigerina [*Spero et al.*, 1997; *Zeebe*, 1999], while there is no obvious reason to expect the epifaunal Cibicidoides to precipitate tests out of equilibrium with seawater. We use the relationship determined from core top measurements of Cibicidoides $\delta^{18}O_{bf}$ over the temperature range 4.1–25.6°C by *Lynch-Stieglitz et al.* [1999]:

$$T = 16.1 - 4.76\left[\delta^{18}O_{bf} - \left(\delta^{18}O_{sw} - 0.27\right)\right]. \quad (1)$$

In this equation and throughout this paper, $\delta^{18}O_{bf}$ values are expressed relative to VPDB and $\delta^{18}O_{sw}$ values are expressed relative to VSMOW; the −0.27‰ adjustment in the equation reflects a combination of the difference between the two scales and the difference in isotopic value obtained from equilibration with water and acid reaction of carbonate [see *Hut*, 1987]. The difference between temperatures calculated using equation (1) and temperatures calculated following *Shackleton* [1974] is small at high $\delta^{18}O$ (low temperature) but larger at low $\delta^{18}O$ (high temperature; Figure 2a), resulting in warmer temperatures calculated for the early Cenozoic in this study compared with previous studies.

[12] Two other factors should be considered in interpreting variations in $\delta^{18}O_{bf}$ over long timescales (≫10 Myr). First, $\delta^{18}O_{sw}$ may vary as a consequence of cycling of water through the lower oceanic crust [*Veizer et al.*, 1999; *Wallmann*, 2001]. Over the last 100 Myr, this process has potentially resulted in an increase in $\delta^{18}O_{sw}$ of 1 ‰ [*Veizer et al.*, 1999; *Wallmann*, 2001, 2004; *Jaffrés et al.*, 2007], although this interpretation is controversial (see discussion by *Jaffrés et al.* [2007]). Second, $\delta^{18}O$ of planktonic foraminifera has been shown to reflect ocean pH as well as temperature and $\delta^{18}O_{sw}$ [*Spero et al.*, 1997] due to construction of foraminiferal tests from dissolved inorganic carbon (DIC), fractionation of oxygen isotopes among the different species of DIC (H_2CO_3, HCO_3^-, and $H_2CO_3^=$), and variation in the equilibrium concentrations of these as a buffer to seawater pH [*Zeebe*, 1999]. Because the pH effect on $\delta^{18}O$ of calcite has a thermodynamic basis, the relationship can be theoretically constrained as a 1.42‰ reduction in $\delta^{18}O$ of calcite for every 1 unit increase in pH [*Zeebe*, 2001]. The actual relationship has been shown to vary among different planktonic foraminiferal species [*Spero et al.*, 1999]. Because of the thermodynamic basis of the pH effect, it is likely to affect all marine carbonates, although this has not been empirically demonstrated in benthic foraminifera

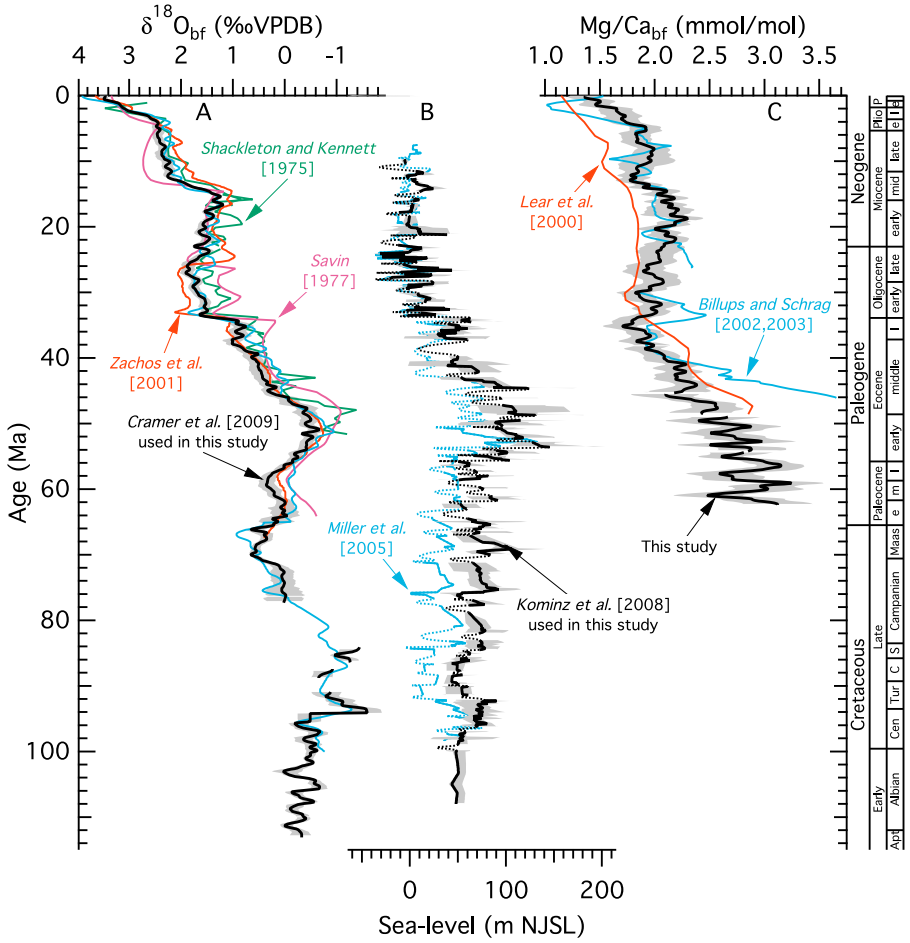

Figure 1. Primary reconstructed proxy records used in this study: (a) $\delta^{18}O_{bf}$, (b) NJSL, and (c) Mg/Ca_{bf}. Records we use are shown in black; prior and alternate versions of these records are shown for comparison. Note the much better correspondence of $\delta^{18}O_{bf}$ trends, as reconstructed by different studies spanning four decades, as compared with Mg/Ca_{bf} in studies spanning only one decade. This reflects the greater difficulty in reconciling Mg/Ca_{bf}, compared with $\delta^{18}O_{bf}$ analyses of different species and from geographic locations. For $\delta^{18}O_{bf}$ (Figure 1a) and Mg/Ca_{bf} (Figure 1c) the 90% confidence envelope is shown, calculated using a bootstrap approach [see *Cramer et al.*, 2009]. For NJSL (Figure 1b) the uncertainty envelope from *Kominz et al.* [2008] is shown, which takes into account the range of sea level estimates from individual core holes in New Jersey. Lowstand NJSL estimates are shown with dotted lines; these estimates are provided by *Kominz et al.* [2008] and *Miller et al.* [2005], but are poorly constrained by data.

[*Zeebe*, 2001]. The deep ocean pH in the past is essentially unconstrained, but assuming the potential for a ~0.5 unit increase in pH since the Cretaceous from modeling results [*Wallmann*, 2004] and that the theoretical relation holds for benthic foraminifera, it is possible that the pH effect has resulted in a ~0.7 ‰ decrease in $\delta^{18}O_{bf}$ since 100 Ma. To the extent that both processes have affected $\delta^{18}O_{bf}$ since the Cretaceous, the pH effect has likely counteracted the effect of water cycling through the crust.

2.2. Mg/Ca_{bf}

[13] We have updated the compilation of Mg/Ca_{bf} measurements shown by *Katz et al.* [2010] and recalculated the Cenozoic trend using different species offsets (see below) (Figures 1 and S1–S3; data compilation and calculated trend are available in the auxiliary material, and published single site records are archived at http://paleoceanDB.net). There are insufficient data from any single ocean basin to calculate basin-specific Mg/Ca_{bf} trends. We use all data that are visually consistent with the available Pacific records in calculating the Mg/Ca_{bf} trend (Figure S1). Significant interbasinal $\delta^{18}O_{bf}$ differences occur only in the Oligocene and Miocene, and primarily with respect to the high latitude Southern Ocean [*Cramer et al.*, 2009], and it should be expected that temperature differences reflected in Mg/Ca_{bf} show the same pattern. For further reassurance, we have calculated a $\delta^{18}O_{bf}$ trend for a selection of individual records equivalent to that used to construct the Mg/Ca_{bf} trend, indicating that there is minimal difference relative to the Pacific basinal trend (Figure S4).

[14] It has been documented that Mg/Ca_{bf} offsets occur among different genera of benthic foraminifera as well as

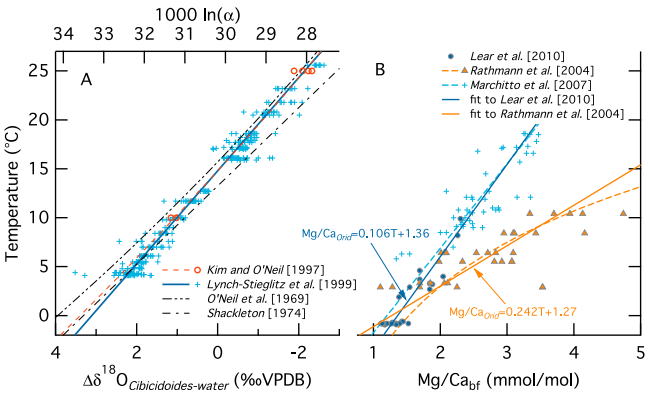

Figure 2. Paleotemperature equations for $\delta^{18}O_{bf}$ and Mg/Ca_{bf}. For $\delta^{18}O_{bf}$ we use the calibration for Cibicidoides of *Lynch-Stieglitz et al.* [1999], which is statistically equivalent to the calibration for inorganic $CaCO_3$ of *Kim and O'Neil* [1997] but results in slightly warmer temperatures at high $\delta^{18}O_{bf}$. The equation traditionally used by paleoceanographers is that of *Shackleton* [1974], who assumed that Cibicidoides precipitated tests with a 0.64‰ offset from equilibrium based on the calibration for inorganic $CaCO_3$ of *O'Neil et al.* [1969]. In consequence, the *Shackleton* [1974] equation diverges from that of *Lynch-Stieglitz et al.* [1999] at high temperatures, although the *O'Neil et al.* [1969] equation for inorganic $CaCO_3$ diverges from that of *Kim and O'Neil* [1997] at low temperatures. For Mg/Ca_{bf} we fit new linear equations to the core top Oridorsalis data sets of *Lear et al.* [2010] and *Rathmann et al.* [2004]; it is not clear why these core top data sets are not compatible with each other. The exponential relationship used by *Rathmann et al.* [2004] and the *Marchitto et al.* [2007] relationship used by *Lear et al.* [2010] are shown for comparison.

among different species of Cibicidoides. Our compilation includes Mg/Ca_{bf} measured on samples of C. wuellerstorfi, C. mundulus, mixed Cibicidoides, Oridorsalis umbonatus, Nuttallides umbonifera, and N. truempyi [*Lear et al.*, 2000, 2003, 2004, 2010; *Billups and Schrag*, 2002, 2003; *Dutton et al.*, 2005; *Shevenell et al.*, 2008; *Sosdian and Rosenthal*, 2009; *Billups and Scheiderich*, 2010; *Dawber and Tripati*, 2011]. There are insufficient data from paired analyses of separate species picked from the same core sample to produce robust fitted calibrations among these different species. Oridorsalis umbonatus analyses are present throughout the time span of the compilation, and we infer offsets between analyses of other species and those of O. umbonatus based on data trends for individual species (Figure S2). Although species offsets in Mg/Ca_{bf} have often been treated as additive, including multiplicative offsets provides a better fit (Figure S2). Published linear temperature calibrations indicate different slopes for the temperature-Mg/Ca_{bf} relationship in different species [e.g., *Elderfield et al.*, 2006; *Bryan and Marchitto*, 2008], which implies that interspecies correction factors should have a multiplicative as well as an additive component.

[15] The influence of Mg/Ca_{sw} variations on Mg/Ca_{bf} ratios is not as straightforward as the relation between $\delta^{18}O_{sw}$ and $\delta^{18}O_{bf}$. Modeled Mg/Ca_{sw} [*Farkaš et al.*, 2007] is consistent with reconstructions from analyses of fluid inclusions in marine evaporites [*Lowenstein et al.*, 2001; *Horita et al.*, 2002], but indicates somewhat higher Mg/Ca_{sw} than analyses of mid ocean ridge flank carbonate veins [*Coggon et al.*, 2010] and fossil echinoderms [*Dickson*, 2002, 2004] (Figure 5b). The model of *Farkaš et al.* [2007] differs from previous models for Mg/Ca_{sw} [*Wilkinson and Algeo*, 1989; *Hardie*, 1996; *Stanley and Hardie*, 1998; *Demicco et al.*, 2005] in that it uses the marine $^{87}Sr/^{86}Sr$ record as an input rather than tectonic reconstructions of seafloor spreading rates. Recent reconstructions of seafloor spreading rates [*Rowley*, 2002; *Cogné and Humler*, 2006; *Müller et al.*, 2008] bear no resemblance to that of *Gaffin* [1987] that has been used as input for Mg/Ca_{sw} reconstructions, and it is questionable whether seafloor spreading rates can be reliably estimated from the spreading history of existing oceanic crust [*Rowley*, 2008].

[16] Studies of Mg/Ca ratios in various calcareous organisms [*Ries*, 2004; *Segev and Erez*, 2006; *Hasiuk and Lohmann*, 2010] indicate that the dependence on Mg/Ca_{sw} generally conforms to the equation

$$Mg/Ca_c = F \cdot Mg/Ca_{sw}^{H}. \quad (2)$$

Previous studies of Mg/Ca_{bf} have followed *Lear et al.* [2000] in multiplying Mg/Ca_{bf} by the ratio of modern Mg/Ca_{sw} to Mg/Ca_{sw} at the time of deposition, effectively assuming H = 1 in equation (2), but to our knowledge this has not been calibrated for deep ocean benthic foraminifera. *Segev and Erez* [2006] cultured shallow water symbiont-bearing benthic foraminifera (Amphistegina lobifera and A. lessonii) and determined values of 0.8 and 0.7 for H, and *Hasiuk and Lohmann* [2010] calculated H = 0.42 for the planktonic foraminifera Globigerinoides sacculifer using data from *Delaney et al.* [1985]. As we show below, it is necessary to assume different values for H depending on the assumed temperature sensitivity for Mg/Ca_{bf}. We ignore uncertainty in the modeled Mg/Ca_{sw} of *Farkaš et al.* [2007] and in the analytical reconstructions of Mg/Ca_{sw} [*Lowenstein et al.*, 2001; *Horita et al.*, 2002; *Dickson*, 2002, 2004; *Coggon et al.*, 2010] because it is not separable at the scale of this study from the uncertainty in the exponent, H, in equation (2).

[17] There is abundant evidence that foraminiferal Mg/Ca reflects the seawater $\Delta[CO_3^{=}]$ as well as temperature and Mg/Ca_{sw} [*Martin et al.*, 2002; *Rosenthal et al.*, 2006; *Elderfield et al.*, 2006; *Yu and Elderfield*, 2008]. *Yu and Elderfield* [2008] calibrated the effect as ~0.009 mmol mol^{-1} $Mg/Ca_{bf}/\mu mol\ kg^{-1}$ $\Delta[CO_3^{=}]$ for C. wuellerstorfi, which is consistent with the inferred relationship from other studies [*Elderfield et al.*, 2006; *Healey et al.*, 2008; *Raitzsch et al.*, 2008]. Multiproxy methods for simultaneous reconstruction of temperature and $\Delta[CO_3^{=}]$ are being developed [*Bryan and Marchitto*, 2008; *Lear et al.*, 2010], but published multiproxy data are not available for most of the records in our compilation. We apply a correction for the $\Delta[CO_3^{=}]$ effect based on the observed decrease in $\Delta[CO_3^{=}]$ with water depth in the modern ocean. The residual values between Mg/Ca_{bf} data from individual sites and the overall trend show a decrease with paleodepth that is consistent with $\Delta[CO_3^{=}]$

data from the modern ocean, in contrast with residual $\delta^{18}O_{bf}$ values that show no trend with paleodepth (Figure S3). This provides supporting evidence for a $\Delta[CO_3^{=}]$ effect on Mg/Ca_{bf} of ~0.009 mmol $mol^{-1}/\mu mol\ kg^{-1}$ and we adjust the Mg/Ca_{bf} data based on a scaled logarithmic fit to the modern $\Delta[CO_3^{=}]$ data:

$$\begin{aligned} Mg/Ca_{bf} &= 0.009\left(\Delta\left[CO_3^{=}\right] - 25\right) \\ \Delta\left[CO_3^{=}\right] &= 47 - 10e^{\left(0.4\,d/1000\right)}, \end{aligned} \tag{3}$$

where d is the paleodepth for the sample. There may be a threshold $\Delta[CO_3^{=}]$ value above which there is little to no effect on Mg/Ca_{bf}, although there is not yet definitive evidence for this in calcareous benthic foraminifera. The offset applied in equation (3) to align Pacific Mg/Ca_{bf} with the global $\Delta[CO_3^{=}]$ regression (Figure S3) is reminiscent of the threshold value of 25 μmol/kg proposed by *Yu and Elderfield* [2008]. Although much of the deep ocean is characterized by $\Delta[CO_3^{=}] < 35$ μmol/mol, we note that our data compilation shows systematic offsets between ocean basins even at shallow depths (where $\Delta[CO_3^{=}] > 35$ μmol) that are most easily explained as reflecting interbasinal differences in $\Delta[CO_3^{=}]$. We correct all of our data, regardless of paleodepth, using equation (3). We do not correct the Mg/Ca_{bf} values for interbasinal differences in $\Delta[CO_3^{=}]$, but when calculating temperatures from Mg/Ca_{bf} we use the CCD reconstruction for the Pacific of *Van Andel* [1975] as a proxy for $\Delta[CO_3^{=}]$ changes through time.

[18] Prior to calculating temperature, the Mg/Ca_{bf} trend must be corrected for the effects of Mg/Ca_{sw} and $\Delta[CO_3^{=}]$ variations through time. We combine equations (2) and (3) to define the corrected Mg/Ca ratio:

$$Mg/Ca_{corr} = \left(Mg/Ca_{bf} - 0.135 \cdot CCD\right) \cdot \left(\frac{5.2}{Mg/Ca_{sw}}\right)^{H}. \tag{4}$$

In our calculations the exponent, H, is set so that when the Mg/Ca_{bf} temperature is used to solve equation (1) for $\delta^{18}O_{sw}$ the result is consistent with minimal ice in the early Eocene. We calculate that melting of all modern ice would lower $\delta^{18}O_{sw}$ from the modern value of 0‰ to −0.89‰ (VSMOW). This is based on the present mass of ocean water (1.39×10^{21} kg; calculated from *Charette and Smith* [2010]), the mass of Antarctic and Greenland ice (2.26×10^{19} kg and 2.66×10^{18} kg; calculated from *Lemke et al.* [2007]), and the mean $\delta^{18}O_{ice}$ for Antarctic and Greenland ice (−52‰ and −34.2‰; *Lhomme et al.* [2005]). The uncertainty in the magnitude of the $\delta^{18}O_{sw}$ decrease with melting of all ice is ~± 0.02‰ (1σ), based on propagating conservative estimates of uncertainty in each of the masses and $\delta^{18}O$ values above, and is therefore negligible in comparison with the other uncertainties involved in our calculations.

[19] Consideration of the thermodynamic effect on the distribution coefficient leads to the expectation of an exponential relationship between Mg/Ca_{bf} and temperature,

$$Mg/Ca_{corr} = B \cdot e^{A \cdot T}, \tag{5}$$

but it has long been recognized that Mg/Ca_{bf} does not conform to this expectation and therefore that the temperature dependence must be mainly due to physiological processes (see discussion by *Rosenthal et al.* [1997]). Many investigators have noted that the Mg/Ca_{bf}-temperature relationship is equally well fit by a linear equation,

$$Mg/Ca_{corr} = A + B \cdot T \tag{6}$$

[e.g., *Lear et al.*, 2002; *Elderfield et al.*, 2006; *Marchitto et al.*, 2007] and that the linear form gives more believable results when extrapolated to low temperatures [*Marchitto et al.*, 2007]. Early calibration studies [*Rosenthal et al.*, 1997; *Martin et al.*, 2002; *Lear et al.*, 2002] were compromised by analytical bias and likely by high-Mg overgrowths (see discussion by *Marchitto et al.* [2007]) and it is questionable whether equations defined only by low-temperature (<5°C) data [e.g., *Yu and Elderfield*, 2008; *Healey et al.*, 2008] can be extended to the higher temperatures that characterize most of the Cenozoic. There is a well-constrained temperature calibration for Cibicidoides pachyderma, with data spanning temperatures of 5.8–18.6°C [*Marchitto et al.*, 2007; *Curry and Marchitto*, 2008], but there are no C. pachyderma measurements in our compilation.

[20] We use two new linear equations fitted to core top O. umbonatus measurements published by *Lear et al.* [2010] (temperature range −0.9–9.9°C) and *Rathmann et al.* [2004] (2.9–10.4°C) (Figure 2b):

$$T = \frac{Mg/Ca_{corr} - 1.36}{0.106} \tag{7a}$$

$$T = \frac{Mg/Ca_{corr} - 1.27}{0.242} \tag{7b}$$

Equations (7a) and (7b) are based on the *Lear et al.* [2010] and *Rathmann et al.* [2004] O. umbonatus data sets, respectively (see section 2.2). It is not clear why these two O umbonatus data sets are incompatible (see Figure 2b). *Lear et al.* [2010] concluded that the *Marchitto et al.* [2007] temperature calibration could be applied to O. umbonatus Mg/Ca_{bf} after subtracting 0.2 mmol/mol based on core top data indicating a relatively low temperature sensitivity for O. umbonatus Mg/Ca_{bf}. To avoid any assumption about the offset between our data and C. pachyderma measurements we use a new linear fit to the O. umbonatus data of *Lear et al.* [2010] (equation (7a); consistent within error with the calibration of *Marchitto et al.* [2007]). Data of *Rathmann et al.* [2004] and *Rathmann and Kuhnert* [2008] indicate a much higher temperature sensitivity for O. umbonatus than that of the *Marchitto et al.* [2007] temperature equation. *Rathmann et al.* [2004] provide an exponential fit for their data, but we find that the core top data are fit equally well by a linear equation (equation (7b)) and that the linear equation results in a more believable Cenozoic temperature history (see section 3). Use of separate calibrations based on the *Lear et al.* [2010] and *Rathmann et al.* [2004] core top data provides a useful illustration of the importance of the Mg/Ca_{bf} sensitivity to Mg/Ca_{sw}. To be consistent with minimal ice volume in the early Eocene the value of H in equation (4) must be different for equations (7a) (H = 0.03) and (7b) (H = 0.70). This is discussed in detail in sections 3 and 4.

2.3. Sea Level

[21] The New Jersey sea level (NJSL) record has been developed using water depth estimates for a network of cored sections from onshore New Jersey [*Miller et al.*, 1998, 2004, 2005]. The most recent update [*Kominz et al.*, 2008] provides an estimate of sea level changes for 10–108 Ma with an error generally ±20 m in less constrained intervals (e.g., the early Miocene) and ±10 m or better in well-constrained intervals (e.g., the Oligocene) and a temporal resolution of ±0.5 Myr to as fine as ±0.1 Myr in some intervals, although gaps (up to ∼2.5 Myr) occur at sea level low-stands. In addition to the analytical error, NJSL as a measure of the change in water thickness attributable to ice sheet growth and decay (SL_{ice}) is subject to systematic uncertainty related to changes in the volume of the global ocean basin (SL_{basin}).

[22] One approach to extracting the SL_{ice} signal would be to independently constrain SL_{basin} and the tectonic history of New Jersey and subtract those components from NJSL. Changes in SL_{basin} can be inferred from ocean crustal production rates (the spreading history of the ocean crust and occurrence of submarine large igneous provinces), but there are major disagreements on the history of global ocean crust production rates and even the sense of SL_{basin} change over the past 100 Myr [see *Rowley*, 2002; *Demicco*, 2004; *Cogné and Humler*, 2006; *Conrad and Lithgow-Bertelloni*, 2007; *Müller et al.*, 2008]. The absence of older crust due to subduction leads to large uncertainties in the SL_{basin} reconstruction for the Paleogene and earlier, and therefore large differences between results from different models. *Rowley* [2008] has argued persuasively that spreading rate histories for no-longer-existing oceanic ridge systems are entirely dependent on model assumptions rather than data. As such, highstands in the NJSL record may provide the best available constraint on SL_{basin} for time periods when continental ice was minimal, although unconstrained tectonic changes in the elevation of New Jersey may be a significant factor [e.g., *Müller et al.*, 2008].

[23] SL_{ice} would reach a maximum of ∼64 m with the melting of all modern ice sheets. This takes into account recent estimates for the volume of grounded ice on Antarctica and Greenland [*Lythe et al.*, 2001; *Bamber et al.*, 2001] (see *Lemke et al.* [2007] for summary), but it does not account for isostatic rebound or alteration of the geoid surface. According to a long-standing assumption, the ∼64 m of extra water thickness would lead to only ∼42 m eustatic sea level rise (i.e., as measured by the NJSL record) due to isostatic compensation involving subsidence of the ocean crust into the mantle under the additional water weight ("Airy" loading; see for instance *Pekar et al.* [2002] and *Miller et al.* [2005]). Considering that growth and decay of large ice sheets involves the transfer of mass between continent-scale land area and the global ocean, the actual crustal response is probably not adequately constrained by a simple Airy loading model. Studies of sea level change since the last glacial maximum (LGM), in response to melting of northern hemisphere ice sheets, imply that whole ocean loading is a minimal effect due to global deformation of the geoid and mantle adjustment, with the result that sea level change during the deglaciation as measured in different locations is widely variable [*Peltier*, 1998; *Peltier and Fairbanks*, 2006; *Raymo et al.*, 2011]. Without a similarly complex model for the far-field effects of Antarctic glaciation, we treat the Airy loading model (42 m) and no loading (64 m) as end-member scenarios constraining the contribution to NJSL change from the growth of ice sheets to modern size.

[24] In intervals where NJSL exceeds these bounds we assume that either SL_{basin} was higher or that the elevation of NJ was tectonically lower than at present. This is the case in the interval older than 34 Ma. A minimal correction would reduce highstands in this interval to 64 m (assuming no isostatic loading effect in NJ) or 42 m (assuming Airy loading in NJ). Such a correction implicitly assumes ice-free conditions during early–middle Eocene highstands, which is a reasonable assumption given that recent paleoclimate model-data integration indicates high latitude surface temperatures >25°C [*Huber*, 2008]. While there is definite evidence for large-scale glaciation of Antarctica starting in the earliest Oligocene (ca. 34 Ma), there is no physical evidence for continent scale ice sheets older than 34 Ma and it is likely from isotopic evidence that essentially ice-free conditions occurred during warm "interglacial" intervals of the Late Cretaceous to Eocene (see discussion by *Miller et al.* [2008]).

[25] We extract SL_{ice} from NJSL by imposing an upper bound on sea level highstands:

$$SL_{ice} = NJSL - \mathrm{LOESS}_{10}[\max_{0.8}(64, NJSL) - 64] \quad (8a)$$

$$SL_{ice} = 1.5 \cdot \{NJSL - \mathrm{LOESS}_{10}[\max_{0.8}(42, NJSL) - 42]\} \quad (8b)$$

where $\max_{0.8}$ indicates the maximum of the values over a 0.8 Myr interval and LOESS_{10} indicates the locally weighted quadratic regression filter originally described by *Cleveland* [1979] as implemented in the software IGOR Pro 6.1 (www.wavemetrics.com) with 10 Myr width. The two forms of the equation are for different treatments of whole-ocean isostatic response: equation (8a) assumes no isostatic subsidence of the ocean floor in response to shifting water from continental ice sheets to the ocean, while equation (8b) assumes water loading leads to isostatic subsidence equivalent to 1/3 of the added water thickness. The LOESS filter is applied so that only variability on long timescales (i.e., the timescales of tectonic processes) is removed, leaving short timescale variability that is most likely attributable to ice-volume changes. Taking the maximum value of NJSL over a 0.8 Myr interval ensures that the correction is adequate to reduce sea level maxima below the 64 m cap (otherwise, the LOESS filter would project a trend through the middle of the data rather than through the highstands we assume are ice-free).

[26] The backstripped NJSL is consistent with other recent sea level records (e.g., Marion Plateau [*John et al.*, 2004, 2011]). Although it is ∼1/3 of the amplitude and differs in detail from the frequently cited Exxon Production Research Company estimates of *Haq et al.* [1987], reviews of new evidence by *Miller et al.* [2005, 2008, 2011] show why the Haq et al. estimates were unrealistically high. The NJSL estimate presented here is also consistent with constraints placed by the size of potential ice-volume budgets. For example, the ∼55 m sea level fall in the earliest Oligocene is consistent with development of an Antarctic ice sheet that is equivalent to the East Antarctic ice sheet today (∼57 m),

with the record of Antarctic glaciation [*Zachos et al.*, 1992; *Barrett*, 1999], and with detailed records from the U.S. Gulf coast [*Katz et al.*, 2008; *Miller et al.*, 2008].

[27] The purpose of extracting SL_{ice} from NJSL is to use it to constrain the $\delta^{18}O_{sw}$ component in $\delta^{18}O_{bf}$, thereby allowing the calculation of deep ocean temperature (see equation (1)). There is a linear relation between changing sea level and $\delta^{18}O_{sw}$:

$$k = \frac{\Delta\delta^{18}O_{sw}}{\Delta SL_{ice}} \tag{9}$$

where k is in units of ‰/m and $\Delta\delta^{18}O_{sw}$ and ΔSL_{ice} are the change in mean isotopic composition of seawater and mean sea level during accumulation or melting of continental ice. Alternatively, k is also related to the mean $\delta^{18}O$ value of continental ice:

$$k = \frac{M_{ice}\left(\delta^{18}O_{sw} - \delta^{18}O_{ice}\right)}{\Delta SL_{ice}\left(M_{sw} + M_{ice}\right)} \approx \frac{\Delta\delta^{18}O_{ice}}{3700} \tag{10}$$

where M_{sw} and M_{ice} are the mass of seawater and mass of ice and 3700 is taken to be the mean depth of the ocean. (The approximation is valid when $|\delta^{18}O_{sw}| \ll |\delta^{18}O_{ice}|$, $\Delta SL_{ice} \ll 3700$ m, and the change in the surface area of the ocean and density of seawater due to accumulation/melting of continental ice is negligible.) A commonly used value for k is −0.011‰/m (corresponding to $\delta^{18}O_{ice} \approx -40$‰), derived by calibrating the glacial-interglacial sea level and $\delta^{18}O$ amplitude in late Pleistocene coral [*Fairbanks and Matthews*, 1978; *Fairbanks*, 1989], although other constraints on glacial-interglacial $\delta^{18}O_{sw}$ amplitude imply a value closer to −0.008‰/m ($\delta^{18}O_{ice} \approx -30$‰) [*Schrag et al.*, 1995; *Waelbroeck et al.*, 2002]. Melting of the present-day East Antarctic, West Antarctic, and Greenland ice sheets (mean $\delta^{18}O_{ice}$ of −56.5‰, −41.1‰, and −34.2‰ [*Lhomme et al.*, 2005]) would yield k of −0.015‰/m, −0.011‰/m, and −0.009‰/m, respectively. These differing values result from varying degrees of fractionation of water during evaporation, transport, precipitation, and incorporation into the ice sheet. Clearly, k should not actually be expected to remain constant through time, but modeling variations in $\delta^{18}O_{ice}$ are beyond the scope of this paper. We use the value −0.011‰/m in our calculations, and return to the topic in the discussion of our results.

3. Calculations and Reconciliation of the Records

[28] In this section, we examine the results from mathematical combination of the $\delta^{18}O_{bf}$, Mg/Ca_{bf}, and NJSL records according to the various hypotheses, models, and constraints discussed in section 2. Some of these lead to implausible results indicating problems with those hypotheses and models. The quality of available data and knowledge of parameters necessary for the calculations are insufficient for determining a uniquely "correct" solution, but the range of results does place constraints on the variation in deep water temperature and ice volume over the last 113 Ma.

[29] We begin the discussion of our results by obtaining our best estimate of ice volume from the NJSL curve, one proxy for ice volume (section 3.1 and Figure 3). We then use this estimate to extract the ice volume component from the Pacific $\delta^{18}O_{bf}$ compilation to yield a deep-sea temperature curve (section 3.2 and Figure 4). We obtain an independent temperature curve from our Mg/Ca_{bf} compilation and use this in combination with the $\delta^{18}O_{bf}$ compilation to extract a $\delta^{18}O_{sw}$ record, an independent proxy for ice volume (section 3.3 and Figure 5). These are compared on a single summary diagram (Figure 6) showing mutual support for some features in the reconstructed temperature and ice volume histories, and we note problems with the underlying data sets that may explain intervals in which the results differ (section 3.4). Special attention is given to the potential implications of this comparison for the temperature and Mg/Ca_{sw} sensitivities of Mg/Ca_{bf} records (section 3.5).

3.1. NJSL

[30] Applying equations (8a) and (8b) to NJSL effectively treats uncorrected NJSL as the best estimate of SL_{ice} for the late Paleogene–Neogene (<~40 Ma) (Figure 3). This is an interval over which crustal production reconstructions are reasonably well constrained [*Rowley*, 2008] and most studies agree that changes in crustal production were small [*Rowley*, 2002; *Müller et al.*, 2008] (but see *Cogné and Humler* [2006]). Our analysis requires a 50–90 m correction during a discreet interval of the early–middle Eocene (55–40 Ma), due to either higher SL_{basin} or tectonic lowering of NJ, or both. The required correction is lower (15–40 m) in the Cretaceous–Paleocene (Figure 3b).

[31] Because we smooth the SL_{ice} record to approximate the smoothing reflected in the $\delta^{18}O_{bf}$ and Mg/Ca_{bf} records the result is significantly affected by the absence of a NJSL estimate at sequence boundaries. We fill the data gaps using the poorly constrained lowstand estimates provided by *Kominz et al.* [2008] as a minimum estimate, linear interpolation as a maximum estimate, and the midpoint between these as the best estimate. The uncertainty envelope for NJSL from *Kominz et al.* [2008] with lowstands filled in this way is applied to the SL_{ice} record in the interval <40 Ma; for the interval >40 Ma the uncertainty envelope is defined by the different SL_{ice} records resulting from equations (8a) and (8b) (Figure 3c). The black curve, with uncertainty envelope, in Figure 3c is used as a reconstruction of SL_{ice} in the discussion below.

[32] In addition to affecting the magnitude of the required adjustment to NJSL, equations (8a) and (8b) lead to substantially different estimates of the magnitude of Myr-scale changes in SL_{ice}. For equation (8a) the magnitude of Myr-scale variations is equivalent to that measured by NJSL. For equation (8b), it is assumed that the whole ocean crust isostatically responds to water loading and consequently the magnitude of Myr-scale variations in NJSL is only 2/3 the magnitude of SL_{ice} changes (SL_{ice} reflects changes in water thickness rather than global sea level). The magnitude of Myr-scale SL_{ice} variations calculated by equation (8b) is 50% larger than those calculated by equation (8a), and would require 50% larger ice sheets. During the Cretaceous–Eocene, that would require accommodating ice sheets as large as 80% of modern, rather than only ~50%, and it would require accommodating ice sheets in the early Oligocene substantially larger than modern rather than roughly equivalent to modern. We find the results and

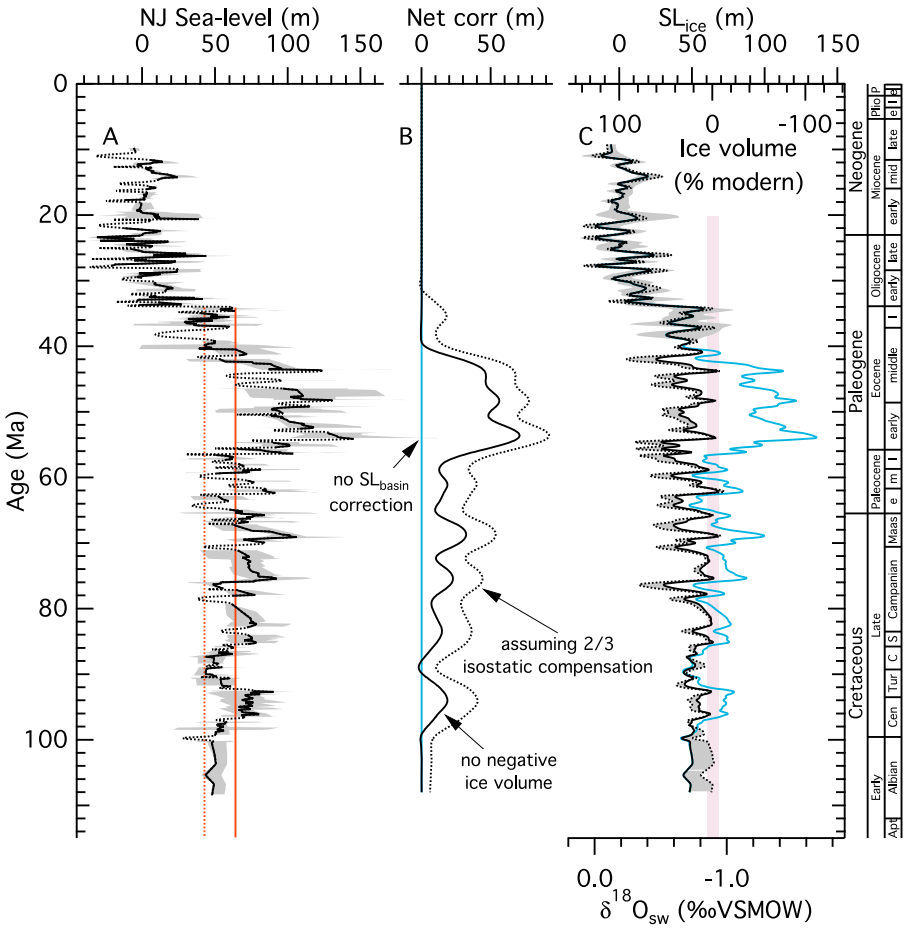

Figure 3. Calculations from the (a) NJSL record to extract (c) SL$_{ice}$. (b) The correction curves are drawn to produce conditions approximating minimal ice during the Late Cretaceous–Eocene in Figure 3c. The solid black line in Figure 3b indicates the correction needed assuming no global ocean basin isostatic response and corresponds with the solid line in Figure 3c; the dotted line indicates correction assuming 1/3 isostatic subsidence and corresponds with the dotted line in Figure 3c. Grey shading in Figure 3c indicates the uncertainty envelope used for further analysis; it is constrained by the uncertainty in NJSL (Figure 3a) and the results from assuming 1/3 isostatic subsidence. The alternate scale for Figure 3c indicates the percentage of modern ice implied by the SL$_{ice}$ curve. The $\delta^{18}O_{sw}$ axis indicates the scaling used to subtract the ice volume effect from $\delta^{18}O_{bf}$ (Figure 4). The scaling used (−0.011‰/m) is not compatible with the mean $\delta^{18}O_{ice}$ for modern ice sheets (see text) so the $\delta^{18}O_{sw}$ value corresponding to 100% of modern ice is not the modern $\delta^{18}O_{sw}$ value.

implications of equation (8a) to be more reasonable, reducing the size of ice sheets that would have to be reconciled with Paleogene warm climates. This suggests that the assumption of a whole ocean adjustment to Airy loading is incorrect [see also *Peltier and Fairbanks*, 2006].

3.2. $\delta^{18}O_{bf}$

[33] Scaling the NJSL-based SL$_{ice}$ record to $\delta^{18}O_{sw}$ (equation (9)) allows a comparison to the Pacific $\delta^{18}O_{bf}$ record and the calculation of deep water temperature via equation (1) (Figure 4). On 10 Myr timescales, the resulting temperature curve shows three warm intervals (early–middle Miocene, early–middle Eocene, and Cenomanian–Campanian) superimposed on a 100 Myr-timescale ~12°C cooling trend from the Late Cretaceous to the Neogene. While the Miocene temperature peak (8 ± 1°C) is clearly cooler than the Eocene (14 ± 2°C), the degree to which high temperatures of the Eocene are cooler than those of the Late Cretaceous is dependent on assumptions about the long-term evolution of $\delta^{18}O_{sw}$ and ocean pH. We treat these two variables independently to delineate extremes for reconstruction of the temperature curve (the two have opposite effects on the calculated temperature, so combination of the two would result in calculated temperatures falling between these extremes). Correcting for the potential pH effect on $\delta^{18}O_{bf}$ (−0.7‰/100 Myr; see section 2.1) implies Late Cretaceous peak temperatures (~20°C; red curve in Figure 4c) substantially higher than Eocene, while correcting for the potential change in $\delta^{18}O_{sw}$ due to cycling of seawater through the crust (+1‰/100 Myr; see section 2.1) results in Late Cretaceous peak temperatures (~13°C; blue curve in Figure 4c) only slightly higher than Eocene. It should be noted that minimal Late Cretaceous $\delta^{18}O_{bf}$ values (peak temperatures) are constrained by analyses from only two

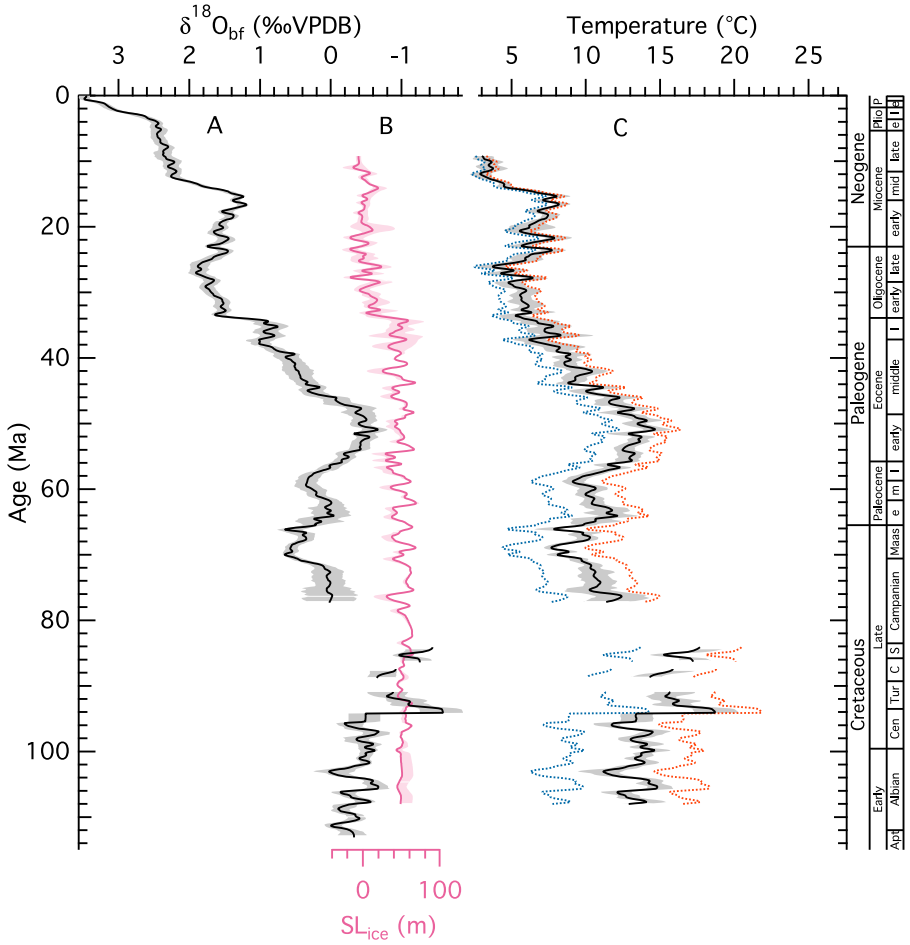

Figure 4. Calculations from (a) the $\delta^{18}O_{bf}$ record and (b) SL_{ice} from Figure 3 to extract deep water temperature. SL_{ice} axis (Figure 4b) is scaled to the $\delta^{18}O_{bf}$ axis (Figure 4a) using −0.011‰/m. (c) Solid black curve gives temperature calculated using the simple difference of the $\delta^{18}O_{bf}$ and SL_{ice} records, with gray shading reflecting the propagation of uncertainty from those two records; blue curve assumes a +1‰/100 Ma gradient in $\delta^{18}O_{sw}$ due to cycling of seawater through the ocean crust; red curve assumes a −0.7‰/100 Ma gradient in $\delta^{18}O_{bf}$ due to changing ocean pH. Because the difference between these end-member solutions is greater than the propagated uncertainty, we use the red and blue curves to constrain the uncertainty on the calculated temperature record.

sites (DSDP Sites 511 and 258); although there is no reason to suspect that these records are severely biased it is possible that a Pacific $\delta^{18}O_{bf}$ record from this interval would show higher values (lower temperatures). In any case, it is not likely that peak Late Cretaceous temperatures were cooler than those of the Eocene, though they may not have been significantly warmer.

3.3. Mg/Ca_{bf}

[34] Combining different assumptions about the various parameters needed to transform Mg/Ca_{bf} into a temperature record allows for a large number of different interpretations. The various resulting temperature records can be used in conjunction with $\delta^{18}O_{bf}$ to produce various $\delta^{18}O_{sw}$ records. Ice volume constraints on $\delta^{18}O_{sw}$ rule out some of these scenarios, but the uncertainty regarding seawater pH and crustal cycling effects on $\delta^{18}O_{bf}$ means that a wide variety of possibilities are still plausible. We discuss end-member scenarios constrained by treating the seawater pH and crustal cycling effects independently (Figure 5), as we did for interpreting $\delta^{18}O_{bf}$ above. We calculate an uncertainty envelope for the temperature trends using the 90% confidence interval for the Mg/Ca_{bf} trend; in the calculation of $\delta^{18}O_{sw}$ the uncertainty envelope also takes into account the 90% confidence interval for the $\delta^{18}O_{bf}$ trend and either a crustal cycling or pH effect on $\delta^{18}O_{bf}$ for maximum and minimum temperature boundaries, respectively.

[35] As noted above, the two temperature equations we consider require different assumptions about the sensitivity of Mg/Ca_{bf} to variations in Mg/Ca_{sw}. The Mg/Ca_{sw} sensitivity required for equation (7b) (H = 0.70 in equation (4)) is similar to values determined for shallow water benthic foraminifera [*Segev and Erez*, 2006], while equation (7a) requires Mg/Ca_{bf} to be essentially insensitive to Mg/Ca_{sw} (H = 0.03). The Mg/Ca_{sw} sensitivity implied by equation (7b) is therefore more plausible in the context of Mg/Ca_{sw}

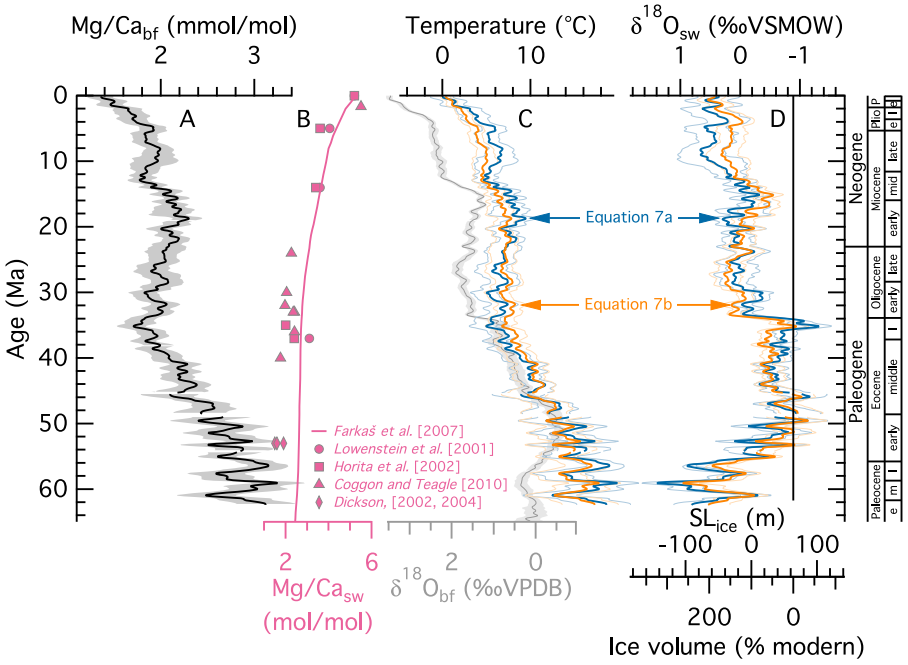

Figure 5. Calculations from the Mg/Ca_{bf} record to extract temperature and $\delta^{18}O_{sw}$ (using $\delta^{18}O_{bf}$ from Figure 4). (a) Mg/Ca_{bf} trend corrected to O. umbonatus. (b) Modeled Mg/Ca_{sw} from *Farkaš et al.* [2007] compared with estimated Mg/Ca_{sw} from fluid inclusions [*Lowenstein et al.*, 2001; *Horita et al.*, 2002], ridge flank carbonate veins [*Coggon et al.*, 2010], and fossil echinoderms [*Dickson*, 2002, 2004]. (c) Calculated temperature and (d) $\delta^{18}O_{sw}$ from equations (7b) and (7a) as discussed in the text. Dotted curves indicate the uncertainty constrained as discussed in the text. Note that the $\delta^{18}O_{sw}$ reconstructed here only reflects variations due to ice volume changes and not changes in $\delta^{18}O_{sw}$ due to crustal cycling. Vertical line in Figure 5d indicates 0 ice volume, used as a primary constraint to evaluate whether the results are reasonable.

sensitivity in other calcareous marine organisms [*Hasiuk and Lohmann*, 2010], but *Stanley et al.* [2005] showed that one species of coccolithophore, Coccolithus neohelis, precipitates coccoliths with Mg/Ca independent of Mg/Ca_{sw} (H = 0), so it is possible that benthic foraminifera are characterized by the low Mg/Ca_{sw} sensitivity implied by equation (7a).

[36] The calculated temperature histories show Paleocene temperatures of 12–20°C gradually cooling to 8–12°C in the middle Eocene (Figure 6). The results from equations (7a) and (7b) diverge beginning in the late middle Eocene, with equation (7a) resulting in a ~4°C cooling to 4–7°C in the early Oligocene and equation (7b) resulting in a smaller ~2°C cooling to 6–9°C. Equation (7a) indicates a slight warming to 7–9°C in the early Miocene while equation (7b) indicates a slight cooling to 6–8°C. Results from equation (7a) indicate a cooling by ~2°C in the middle Miocene followed by a ~1°C warming in the late Miocene; the cooling is of smaller magnitude for equation (7b) (~1°C) and subsequent warming is negligible. Cooling during the late Miocene–Pliocene leads to Pleistocene temperatures of ~0°C, with a larger uncertainty for equation (7a) (−1–2°C) than for equation (7b) (0–1°C). The discrepancy between the results for equations (7a) and (7b) in the middle Eocene–early Miocene reflects the different temperature and Mg/Ca_{sw} sensitivities. Temperature decreases more gradually with Mg/Ca_{bf} in equation (7b) than in equation (7a), so the middle Eocene cooling is of smaller magnitude; equation (7a) requires low Mg/Ca_{sw} sensitivity so that less of the Oligocene–middle Miocene Mg/Ca_{bf} increase is attributed to the coincident Mg/Ca_{sw} increase.

[37] When combined with $\delta^{18}O_{bf}$, results from both equations (7a) and (7b) indicate ice volume decreasing from ~200% of modern in the Paleocene to ~10% in the early Eocene; large ~2 Myr oscillations in this interval would require accumulation and melting of the equivalent of the modern Antarctic ice sheet. We know of no evidence for continent-scale Antarctic ice sheets during the early Paleogene, so we consider the Paleocene results and the amplitude of oscillations in the early Eocene to be unreasonable. The large 2–5 Myr oscillations in Mg/Ca_{bf} in the Paleocene–early Eocene are most likely a consequence of aliasing higher frequency variability: the transition from high amplitude to more subdued oscillations is coincident with a change from low- to high-resolution sampling for the Site 1209 record (Figure S1). Following an increase in ice volume to ~50% of modern in the middle Eocene, results for the two equations diverge: equation (7b) indicates a decrease to 0% modern ice volume in the late Eocene and an abrupt increase at the Eocene/Oligocene boundary to ~140% of modern ice volume; results from equation (7a) indicate a decrease to negative ice volume (clearly unreasonable) in the late Eocene followed by an abrupt increase at the E/O boundary to ~100% of modern ice volume. Increasing ice volume during the Oligocene for equation (7a) and a late Oligocene decrease in ice volume for equation (7b) leads to

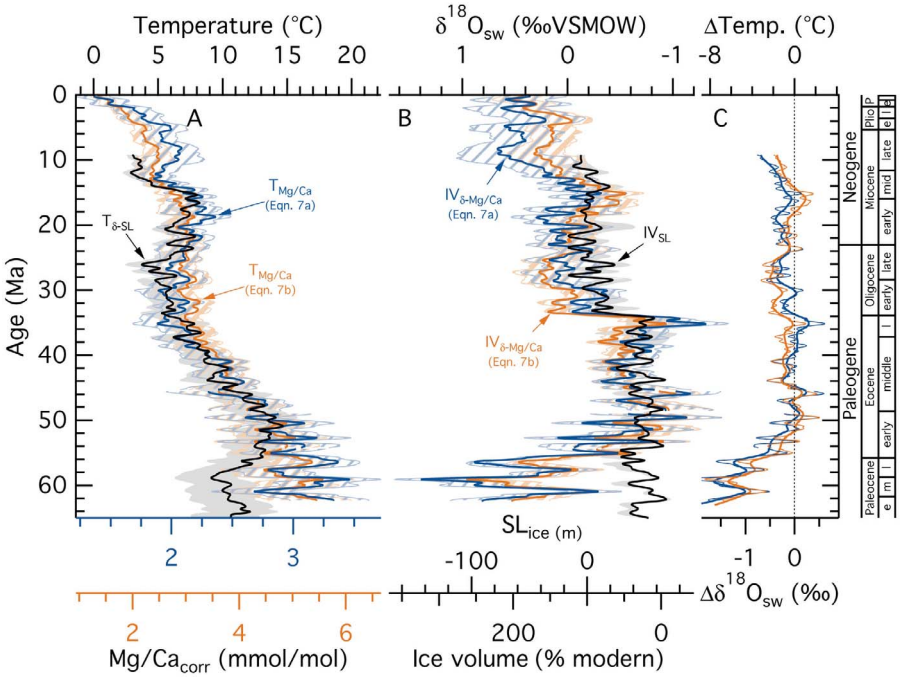

Figure 6. Comparison of (a) temperature ($T_{\delta-SL}$ and $T_{Mg/Ca}$) and (b) ice volume (IV_{SL} and $IV_{\delta-Mg/Ca}$) reconstructions resulting from the manipulations in Figures 3–5. The gray shaded region in Figure 6a is constrained by the blue and red curves in Figure 4c (not the same as the gray shaded region in Figure 4c). The gray shaded area in Figure 6b is the same as the gray region shown in Figure 3c. Colored lines in Figures 6a and 6b as in Figure 5; the uncertainty for these curves (region between dotted orange and blue lines in Figure 5) are shown as blue and orange hatched regions. Alternate axes show the Mg/Ca_{corr} values (equation (4)) for each $T_{Mg/Ca}$ calculation and correspond with the values on the Mg/Ca_{corr} axis shown in Figure 7. (c) Differences between temperature/$\delta^{18}O_{sw}$ reconstructions, with smoothed versions as discussed in the text. The difference curves for temperature and $\delta^{18}O_{sw}$ are identical except for scaling. Reconstructions of $\delta^{18}O_{sw}$ exclude changes due to cycling of water through the crust. Reconstructions shown in Figures 6a and 6b are available as tabulated data in the auxiliary material.

a crossover of the results: results from equation (7a) indicate greater ice volume in the early Miocene (~140%) than results from equation (7b) (~120%). The results indicate a decrease in ice volume from the early to middle Miocene (to ~100% for equation (7a) and ~60% for equation (7b)), and increase from the middle to late Miocene (to ~200% for equation (7a) and ~160% for equation (7b)). Gradually decreasing ice volume for equation (7a) (overprinted by 2–5 Myr oscillations) and a late Pliocene increase in ice volume for equation (7b) leads to convergence of the results at ~190% of modern ice volume in the Pleistocene. The mean Pleistocene ice volume is expected to be between interglacial and glacial extremes. Considering that the ~120 m sea level lowering at the last glacial maximum [*Peltier and Fairbanks*, 2006] indicates ice volume ~280% of modern, ~190% is reasonable for the mean Pleistocene state.

[38] In summary, the ice volume results suggest that our Mg/Ca_{bf}-based temperature reconstruction yields temperatures that are too high in the Paleocene, that the amplitude of variability in the early Eocene is too large, and that the late Eocene temperatures for equation (7a) are too low. Results from equation (7b) show the expected increase in ice volume in the late Pliocene–Pleistocene. Results from equation (7a) instead indicate greater ice volume in the late Miocene than in the Pleistocene, implying that the Mg/Ca_{bf}-based temperature results from equation (7a) are too high in the late Miocene.

3.4. Comparison of Results

[39] The calculations above provide two largely independent approaches to deriving deep water temperature and ice volume: one using ice volume approximated from sea level to extract temperature from $\delta^{18}O_{bf}$, and another using temperature calculated from Mg/Ca_{bf} to extract ice volume from $\delta^{18}O_{bf}$ (Figure 6) (for brevity in the subsequent discussion we use subscripts as a shorthand describing the underlying data used for the different approaches: $IV_{SL}/T_{\delta-SL}$ and $IV_{\delta-Mg/Ca}/T_{Mg/Ca}$). The two approaches, as implemented here, are not fully independent: because of uncertainties about the necessary parameters we have forced all the records calculated here to produce essentially ice-free conditions in the early Eocene. That constraint in the early Eocene should not affect the timing of cooling and ice sheet growth through the late Paleogene and Neogene, and we consider the concordance of results from the two approaches over this interval as supporting evidence that the underlying models are sound. Variability at timescales >3 Myr is well correlated between results from the two approaches; the correlation is less good at timescales <3 Myr, but is statistically significant at >95% confidence for both temperature

and ice volume reconstructions at all timescales >1 Myr (Figure S5).

[40] We stress that our observations are not applicable to Myr-scale variations, which have been filtered out of these records. For instance, a number of studies have addressed the apparent incompatibility of sea level, $\delta^{18}O_{bf}$, and Mg/Ca_{bf} records in the earliest Oligocene [*Lear et al.*, 2000, 2004, 2008; *Billups and Schrag*, 2003; *Coxall et al.*, 2005; *Katz et al.*, 2008]. Our results indicate that the long-term shift in the mean cryosphere state that occurred near the Eocene/Oligocene boundary was not accompanied by a similarly abrupt shift in the long term mean deep ocean temperature, but that has very little relevance to the relative contribution of ice growth and temperature change during the much larger (>1.0‰), transient (<300 kyr) $\delta^{18}O_{bf}$ event in the earliest Oligocene (Oi-1).

[41] Our reconstructions indicate a gradual decline in temperature during the Eocene, from 14 ± 3°C in the early Eocene to 6 ± 2°C in the late Eocene. The $\delta^{18}O_{bf}$–sea level approach ($T_{\delta-SL}$) (black line and gray shaded area in Figure 6a) indicates a further ~2°C cooling during the Oligocene followed by a ~3°C warming in the late Oligocene–early Miocene, while the Mg/Ca_{bf} approach ($T_{Mg/Ca}$) (orange and blue lines and hatched areas in Figure 6a) indicates either a slight warming or essentially stable temperatures through this interval, depending on the value of H. The magnitude of the cooling during the middle Miocene is larger for $T_{\delta-SL}$ (~4°C) than for $T_{Mg/Ca}$ (2–3°C).

[42] Both approaches indicate an abrupt increase in ice volume at the Eocene/Oligocene boundary (Figure 6b); the magnitude of this shift is greater for the $\delta^{18}O_{bf}$–Mg/Ca_{bf} approach ($IV_{\delta-Mg/Ca}$) than for the NJSL approach (IV_{SL}) (change equivalent to ~110% vs ~60% of modern ice volume). During the Oligocene–early Miocene all results indicate ice volume in the range 60–140% of modern, although results differ in showing a gradual increase in ice volume through this interval (IV_{SL} and equation (7a) $IV_{\delta-Mg/Ca}$) or a late Oligocene–early Miocene decrease (equation (7b) $IV_{\delta-Mg/Ca}$). It is worth noting that topographic reconstruction of the Antarctic landscape for 34 Ma indicates that land area was 10–20% greater than has been assumed [*Wilson and Luyendyk*, 2009] (updated to 18–24% greater by *Wilson et al.* [2011]), and hence could accommodate a substantially larger ice sheet.

[43] The largest discrepancy between the two approaches occurs in the Paleocene–early Eocene, with lesser discrepancies in the late Miocene and late Eocene (Figure 6). In section 4.1 we examine the potential implications of the discrepancies for geologically interesting parameters: Mg/Ca_{sw}, $\delta^{18}O_{ice}$, and $\Delta[CO_3^{=}]$. However, the discrepancies may instead simply reflect problems with the underlying data that we discuss here.

[44] The Paleocene–early Eocene Mg/Ca_{bf} record is primarily constrained by a single record, from ODP Site 1209 (Shatsky Rise, western Pacific [*Dutton et al.*, 2004, 2005]), with data from ODP Site 689 (Weddell Sea, Southern Ocean [*Lear et al.*, 2000; *Billups and Schrag*, 2003]) in only a short interval ~55 Ma. Moreover, the ODP Site 1209 record is constrained almost exclusively by analyses of Nuttalides truempyi in the interval >53 Ma; the Mg/Ca for the single O. umbonatus analysis in this interval (~58 Ma) is low relative to the corrected N. truempyi measurements and consistent with the lower temperature indicated by the $T_{\delta-SL}$ reconstruction. N. truempyi may have a different sensitivity to Mg/Ca_{sw} than O. umbonatus; alternatively, N. truempyi is an infaunal species and may not have a consistent offset relative to O. umbonatus due to changes in pore water chemistry. In their discussion, *Dutton et al.* [2004] provide good arguments against potential explanations for the discrepancy between this record and $\delta^{18}O_{bf}$ variations: diagenesis, variable Mg/Ca_{sw}, ice volume, seawater pH, and interbasinal $\delta^{18}O_{sw}$ variations. We explore the potential for Mg/Ca_{sw} changes in section 4.1, but stress that the Paleocene–early Eocene Mg/Ca_{bf} trend needs to be confirmed before concluding that one, or some combination, of these unlikely scenarios must be true. There is some support for the trend we show from a tropical Pacific planktonic foraminiferal Mg/Ca record that similarly indicates stable Mg/Ca values during this interval of increasing $\delta^{18}O$, although those values may be explained by diagenetic recalcification of planktonic foraminifera [*Tripati et al.*, 2003].

[45] In the middle Miocene, both approaches indicate a temperature decrease and ice volume increase, but the $T_{\delta-SL}$ decrease is larger than in $T_{Mg/Ca}$ and the IV_{SL} increase is smaller than in $IV_{\delta-Mg/Ca}$. There are reasons to question both the Mg/Ca_{bf} and the NJSL record in this interval. The bias in NJSL toward interglacial sea level highstands is expected to increase as the amplitude of ice volume changes increases. Offshore drilling by IODP Expedition 313 [*Expedition 313 Scientists*, 2010] has targeted lower-middle Miocene lowstand deposits that are not represented onshore and it is clear that the early middle Miocene eustatic estimates from onshore NJ are strongly biased to highstands [*Miller et al.*, 2005; *Kominz et al.*, 2008]. For example, on the Marion Plateau, eustatic falls during late middle Miocene were backstripped as ~55 m, versus ~40 m in New Jersey at this time [*John et al.*, 2004]. The Mg/Ca_{bf} record suffers from lack of continuous records through this interval (Figure S2a). The constraint on the early Miocene Mg/Ca_{bf} peak is limited to a record from Site ODP 747; the trend for ODP 747 in the middle Miocene–Pleistocene does not match any of the other records but we include the late Oligocene–early Miocene portion because no other records are available (Figure S1). The middle Miocene Mg/Ca_{bf} minimum occurs at the young end of the record from ODP Site 1171 (Pacific sector Southern Ocean) and the old end of the record from ODP Site 806 (western Equatorial Pacific); the record from ODP Site 926 (western Equatorial Atlantic) is continuous through this interval, but we have excised the late Miocene interval of this record because it shows a warming not present in the Pacific (Figure S2a) [see *Billups and Scheiderich*, 2010].

3.5. Mg/Ca_{bf} Sensitivity to Temperature and Mg/Ca_{sw}

[46] There is a clear linear correlation between Mg/Ca_{corr} (equation (4)) and $T_{\delta-SL}$, if we ignore the interval >53 Ma that is constrained only by Site 1209 N. truempyi analyses (Figure 7). It is possible that an exponential temperature dependency could explain the data >57 Ma, which would then leave the data 45–57 Ma as anomalously low in Mg/Ca_{corr}, but we believe it is more plausible that the Paleocene N. truempyi Mg/Ca_{bf} data are anomalously high. Clearly, the exponential fit to core top O. umbonatus data of *Rathmann et al.* [2004] cannot explain the correlation we

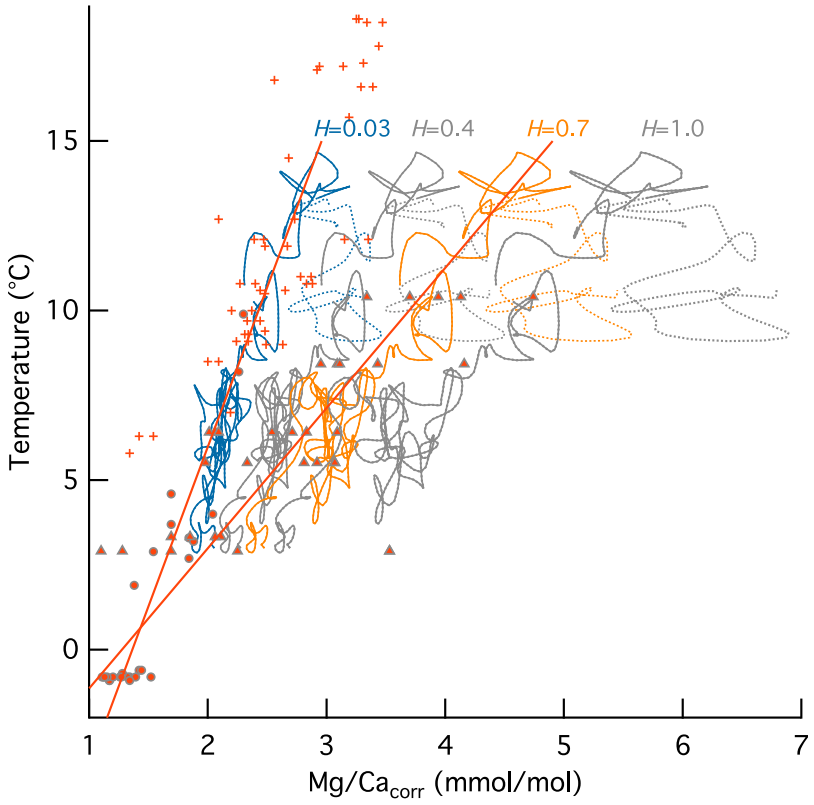

Figure 7. Correlation between $T_{\delta-SL}$ (Figures 4c and 6a) with Mg/Ca_{corr} (equation (4) and Figure 6a) calculated using various values for H, as labeled. Core top data and fitted temperature relationships as in Figure 2b are shown for comparison. The blue (H = 0.03) and orange (H = 0.70) curves correspond with equations (7a) and (7b), respectively, and show the correlation of the black $T_{\delta-SL}$ curve with the blue and orange Mg/Ca_{corr} curves from Figure 6a. The plot illustrates the correspondence of these with core top data from *Lear et al.* [2010] and *Rathmann et al.* [2004]. Interval >53 Ma is shown dotted, as we suspect that the Mg/Ca_{bf} trend in this interval is not accurate.

observe with or without the data >57 Ma (compare Figures 2 and 7).

[47] Because temperature decreases and Mg/Ca_{sw} increases through the Cenozoic, there is a tradeoff in this data between the temperature sensitivity and Mg/Ca_{sw} sensitivity of Mg/Ca_{bf}: assuming high (low) temperature sensitivity requires high (low) Mg/Ca_{sw} sensitivity and vice versa. The Cenozoic record conforms well to the high temperature sensitivity of the *Rathmann et al.* [2004] core top O. umbonatus data if a high Mg/Ca_{sw} sensitivity (H = 0.70 in equation (4)) is assumed, but it also conforms well to the low temperature sensitivity of the *Lear et al.* [2010] O. umbonatus data and the *Marchitto et al.* [2007] C. pachyderma data if a low Mg/Ca_{sw} sensitivity is assumed (H = 0.03 in equation (4)) (Figure 7). As noted above, a high Mg/Ca_{sw} sensitivity for benthic foraminifera is consistent with most of the marine organisms for which the sensitivity is known [*Hasiuk and Lohmann*, 2010]; our results show that a high Mg/Ca_{sw} sensitivity is inconsistent with data indicating a low temperature sensitivity for modern benthic foraminifera [*Marchitto et al.*, 2007; *Bryan and Marchitto*, 2008].

[48] It is likely that different species of benthic foraminifera have different sensitivities to Mg/Ca_{sw}. *Segev and Erez* [2006] determined different sensitivities for two different species of the shallow water genus Amphistegina (H = 0.7 for A. lessonii and H = 0.8 for A. lobifera) while *Stanley et al.* [2005] demonstrated that different genera of coccolithophores can have extremely different Mg/Ca_{sw} sensitivities (H = 0.9 for Pleurochrysis carterae, H = 1.5 for Ochrosphaera neopolitana, and H = 0.0 for Coccolithus neohelis; values calculated by *Hasiuk and Lohmann* [2010]). If the Mg/Ca_{bf} differences among species in part reflects different sensitivities to Mg/Ca_{sw} then the offsets among species should not be expected to be constant through the Cenozoic. The large difference between analyses of Nuttalides and those of Oridorsalis and Cibicidoides (Figure S2) may reflect a large difference in Mg/Ca_{sw} sensitivity, which could contribute to the discrepancy between the $T_{Mg/Ca}$ and $T_{\delta-SL}$ reconstructions in the Paleocene. There is supporting evidence for a difference in Mg/Ca_{sw} sensitivity between Nuttalides and Oridorsalis in a much larger difference between N. umbonifera and O. umbonatus analyses observed in the early Oligocene (DSDP Site 522) compared to the Neogene (Sites DSDP 573 and ODP 926). We do not observe a variation in the offset among O. umbonatus, C. mundulus, and C. wuellerstorfi Mg/Ca_{bf} during the Neogene, when

Mg/Ca_{sw} changes are large, so these species most likely have similar Mg/Ca_{sw} sensitivities (a more robust data set of paired analyses would be required to entirely rule out differences in Mg/Ca_{sw} sensitivity among these species). The problem is further complicated by the need to correct Mg/Ca_{bf} measurements for $\Delta[CO_3^{=}]$ variations and the potential that different species respond differently to $\Delta[CO_3^{=}]$.

[49] Reconstructing Cenozoic temperatures using Mg/Ca_{bf} requires knowing not only the Cenozoic variation in Mg/Ca_{sw} but also the Mg/Ca_{bf} sensitivity to Mg/Ca_{sw}. The difficulty of culturing deep sea benthic foraminifera may prevent laboratory determination of the Mg/Ca_{sw} sensitivity for most species [see, e.g., *Filipsson et al.*, 2010]. With adequate constraint on the temperature sensitivity and Mg/Ca_{sw}, the correlation between corrected Mg/Ca_{bf} and $T_{\delta-SL}$ demonstrated here can provide some constraint on Mg/Ca_{sw} sensitivities.

4. Discussion

[50] We undertook the analysis presented here with the intention of testing the hypothesis that NJSL and Mg/Ca_{bf} are robust climate proxy records for long-timescale variations in global ice volume and deep ocean temperature, respectively. By combining these two proxies with $\delta^{18}O_{bf}$, which reflects a combination of ice volume and temperature effects, we have generated separate records of deep ocean temperature and $\delta^{18}O_{sw}$ that overlap from the Paleocene–Miocene. Except at the ends of this overlapping interval, the separate records are consistent within ±2°C temperature, a difference that is similar in magnitude to the uncertainty in the Mg/Ca_{bf} trend calculation (equivalently, the consistency can be stated as ±0.4‰ $\delta^{18}O$, ±60% modern ice volume, or ±35 m sea level). Variability in the separate reconstructions is correlated over all timescales >1 Myr (confidence >95%; Figure S5), confirming that the visually apparent concordance is not a consequence of the imposed temperature decrease since the early Eocene. Our analysis, therefore provides significant support to the use of these records as proxies for climate change through the Cenozoic, and we argue that these reconstructions provide fundamental insight into the >5 Myr variability in deep ocean temperature and ice volume through the Cenozoic.

[51] There are also obvious discrepancies between the derived temperature and ice volume records. As discussed in the previous section, there are potential problems with the underlying data that may account for these discrepancies, but it is also possible that these discrepancies reflect variations in parameters that are more interesting from a geologic perspective. In the following sections we explore the potential implications of interpreting the discrepancies as reflecting variations in Mg/Ca_{sw}, $\delta^{18}O_{ice}$, or $\Delta[CO_3^{=}]$, and then discuss how these records may change our view of Cenozoic cooling.

4.1. Mg/Ca_{sw}, $\delta^{18}O_{ice}$, and $\Delta[CO_3^{=}]$

[52] The difference between temperature reconstructions ($T_{\delta-SL}$ and $T_{Mg/Ca}$) or between ice volume reconstructions (IV_{SL} and $IV_{\delta-Mg/Ca}$) can be used to reconstruct variations in Mg/Ca_{sw}, $\delta^{18}O_{ice}$, or $\Delta[CO_3^{=}]$ (Figure 8); we assume the CCD-based correction for $\Delta[CO_3^{=}]$ when calculating Mg/Ca_{sw} and $\delta^{18}O_{ice}$, the *Farkaš et al.* [2007] reconstruction of Mg/Ca_{sw} when calculating $\Delta[CO_3^{=}]$ and $\delta^{18}O_{ice}$, and a constant $\delta^{18}O_{ice}$ of ∼−40‰ (k = −0.011 in equation (10)) when calculating Mg/Ca_{sw} and $\Delta[CO_3^{=}]$. For Mg/Ca_{sw},

$$Mg/Ca_{sw} = 5.2\left(\frac{Mg/Ca_{bf} - 0.135 \cdot CCD}{0.242 \cdot T_{\delta-SL} + 1.27}\right)^{1/H} \quad (11)$$

where 5.2 mol/mol is the modern Mg/Ca_{sw}. Note that it is not possible to calculate Mg/Ca_{sw} when H ≈ 0, as is required for equation (7a); equation (11) is based on equation (7b). For $\delta^{18}O_{ice}$,

$$\delta^{18}O_{ice} = 3700\left(\frac{-1.17 - \delta^{18}O_{sw}}{64 - SL_{ice}}\right), \quad (12)$$

where 3700 m is the mean depth of the ocean, −1.17 and 64 are the $\delta^{18}O_{sw}$ and SL_{ice} with no ice, and $\delta^{18}O_{sw}$ is calculated using Mg/Ca_{bf} to constrain temperature (equations (7a) and (7b)) and solving equation (1) for $\delta^{18}O_{sw}$. For $\Delta[CO_3^{=}]$,

$$\Delta[CO_3^{=}] = \frac{1}{0.009}\left[Mg/Ca_{bf} - (1.36 + 0.106 \cdot T_{\delta-SL})\left(\frac{Mg/Ca_{sw}}{5.2}\right)^{H}\right], \quad (13a)$$

$$\Delta[CO_3^{=}] = \frac{1}{0.009}\left[Mg/Ca_{bf} - (1.27 + 0.242 \cdot T_{\delta-SL})\left(\frac{Mg/Ca_{sw}}{5.2}\right)^{H}\right], \quad (13b)$$

Equations (13a) and (13b) correspond with temperature equations (7a) and (7b) respectively. We make these calculations using curves filtered to remove variations at <5 Myr wavelength. Variations in $\delta^{18}O_{ice}$ and $\Delta[CO_3^{=}]$ may contribute to the lack of coherence among the records at shorter wavelength, but we do not have sufficient confidence in the available records to attempt to interpret these variations (see section 3.4 and Figure S5). The Mg/Ca_{sw} reconstruction is further smoothed because Mg/Ca_{sw} is not expected to vary rapidly due to the long residence time for Mg in the ocean. Rendering the differences between reconstructions in these ways (Figure 8) is perhaps most useful in indicating intervals in which other factors must be involved, such as the data problems discussed in section 3.4. We evaluate these by comparing the Mg/Ca_{sw} reconstruction with estimates from fluid inclusions and with crustal production reconstructions, by comparing the $\delta^{18}O_{ice}$ reconstruction with the modern end-member values for the East Antarctic ice sheet (−57 ‰) and the Greenland ice sheet (−34 ‰ [*Lhomme et al.*, 2005]), and by comparing the $\Delta[CO_3^{=}]$ reconstruction with changes in the CCD. The values of all these reconstructions can be shifted by assuming different values for the Mg/Ca_{bf} sensitivity to Mg/Ca_{sw} (H in equation (4)); these reconstructions may therefore provide some insight whether equation (7a) or (7b) is more realistic.

4.1.1. Mg/Ca_{sw}

[53] As noted above, it is not possible to calculate Mg/Ca_{sw} using results from equation (7a). The results from equation (7b) indicate Mg/Ca_{sw} values similar to that

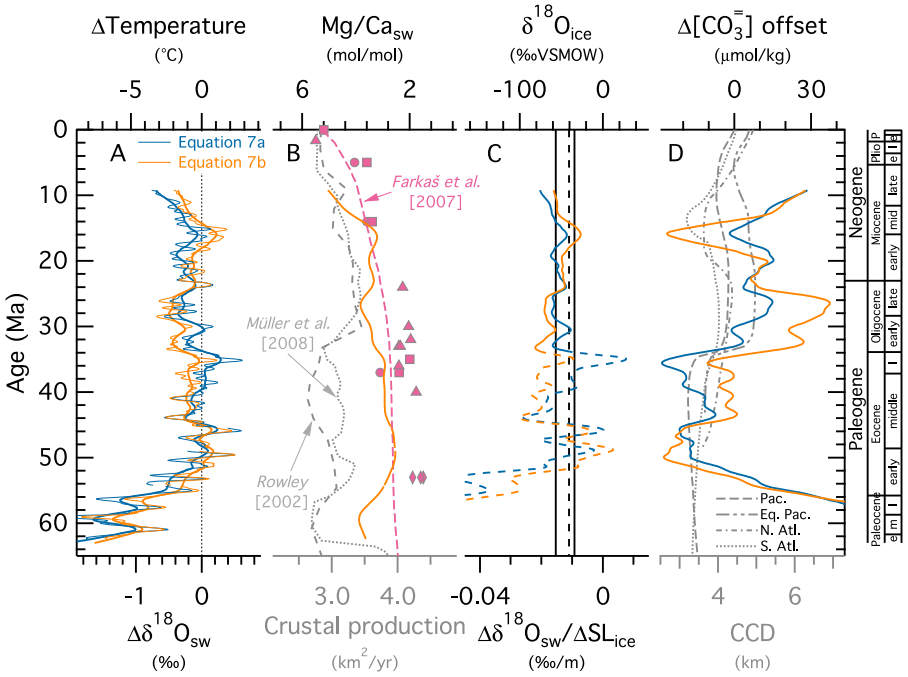

Figure 8. (a) Difference curves from Figure 6c. (b) Variations in Mg/Ca_{sw} implied by the difference curve in Figure 8a (equation (11)), compared with the modeled Mg/Ca_{sw} of *Farkaš et al.* [2007] and measured values for Mg/Ca_{sw} (symbols as in Figure 5). Crustal production reconstructions are also shown, because crustal production is a primary control on Mg/Ca_{sw}. (c) Variations in $\delta^{18}O_{ice}$ (also scaled as $\Delta\delta^{18}O_{sw}/\Delta SL_{ice}$) implied by the difference curve in Figure 8a (equation (12)). Vertical solid black lines indicate the value of the modern east Antarctic ice sheet (−56.5‰) and Greenland ice sheet (−34.2‰); vertical dashed line indicates the value used in the reconstructions shown in Figures 3–6 (−0.011‰/m) applicable to ice volume changes since the LGM and also equivalent to the value of the modern west Antarctic ice sheet. (d) Variations in $\Delta[CO_3^{=}]$ implied by the difference curve in Figure 8a (equation (13a)) compared with variations in the CCD for different ocean basins from *Van Andel* [1975].

modeled by *Farkaš et al.* [2007] except in the Paleocene, late Oligocene, and late Miocene (Figure 8b). High Mg/Ca_{sw} reconstructed in the late Miocene and late Oligocene is not compatible with either the *Farkaš et al.* [2007] model or data from fluid inclusions [*Lowenstein et al.*, 2001; *Horita et al.*, 2002]. High Mg/Ca_{sw} values in the Paleocene, gradually decreasing to the early Eocene, are also not compatible with the *Farkaš et al.* [2007] model, but there are no analytical data to compare with in this interval. Crustal production reconstructions [*Rowley*, 2002; *Müller et al.*, 2008] show an increase in the late Paleocene that might account for such a decrease in Mg/Ca_{sw}. Likewise, the increase in NJSL to anomalously high levels in this interval could be accounted for by a significant increase in crustal production rates affecting SL_{basin} (Figure 3). We note a slight similarity between the equation (7b) Mg/Ca_{sw} reconstruction and the crustal production reconstruction of *Müller et al.* [2008]: Mg/Ca_{sw} minima at ∼16 Ma, ∼36 Ma, and ∼50 Ma lag crustal production maxima, as would be expected due to the long residence time for Mg.

4.1.2. $\delta^{18}O_{ice}$

[54] We attempt to interpret reconstructions of $\delta^{18}O_{ice}$ only for the Oligocene–Miocene; in the Paleocene–Eocene the $\delta^{18}O_{ice}$ reconstructions are erratic due to low ice volume (i.e., the denominator in equation (12) is near 0; Figure 8). Results from equation (7a) indicate $\delta^{18}O_{ice}$ in the range of the modern Antarctic ice sheet in the Oligocene–middle Miocene; results from equation (7b) indicate an increase in the $\delta^{18}O_{ice}$ from values slightly lower than the modern East Antarctic ice sheet in the early Oligocene to values slightly higher than the modern Greenland ice sheet in the middle Miocene. The equation (7a) $\delta^{18}O_{ice}$ reconstruction is consistent with an expectation that the dynamic Oligocene ice sheet [*Naish et al.*, 2001; *Barrett*, 2007] had composition varying between that of the modern polar East Antarctic ice sheet and the more temperate modern West Antarctic ice sheet and LGM northern hemisphere ice sheet. The equation (7b) reconstruction instead implies that the ice sheet composition was similar to the modern East Antarctic ice sheet in the early Oligocene, shifting toward the modern Greenland composition in the early–middle Miocene. This is possibly consistent with measurements indicating lower $\delta^{18}O$ in precipitation during the greenhouse climate of the Cretaceous [*White et al.*, 2001], and would make it easier to explain the magnitude of the early Oligocene $\delta^{18}O$ increase (Oi-1 [see *Katz et al.*, 2008]). Both equations (7a) and (7b) indicate a decrease in $\delta^{18}O_{ice}$ during the middle Miocene, consistent with the transition to a stable, cold ice sheet at this time [*Lewis et al.*, 2007, 2008; *Bertler and Barrett*, 2010], but the increase is of larger magnitude than can be explained by the range between modern Greenland and Antarctic ice sheet $\delta^{18}O_{ice}$ (equation (7a) indicates late Miocene $\delta^{18}O_{ice}$ lower than that of the modern Antarctic ice sheet while

equation (7b) indicates middle Miocene $\delta^{18}O_{ice}$ higher than that of the modern Greenland ice sheet).

4.1.3. $\Delta[CO_3^{=}]$

[55] The $\Delta[CO_3^{=}]$ reconstructions show an increase in the late Eocene–early Oligocene more than twice as large as the increase we assumed based on the Pacific CCD reconstruction of *Van Andel* [1975]. The reconstruction based on equation (7a) continues to increase gradually through the early Miocene; the reconstruction based on equation (7b) instead shows a decrease from the late Oligocene–early Miocene that is more consistent with the *Van Andel* [1975] reconstruction of the CCD for the Atlantic basin, although again of much larger magnitude (note that the shallowing of the Atlantic CCD in this interval is very poorly constrained [*Berger and von Rad*, 1972]). The increase in $\Delta[CO_3^{=}]$ during the middle Miocene is consistent with the results of *Lear et al.* [2010] based on paired Li/Ca and Mg/Ca analyses from the Indian Ocean (Site 761), but the *Lear et al.* [2010] reconstruction indicates a peak at ~14 Ma with a subsequent decrease while our calculations indicate continued increase into the late Miocene. *Billups and Scheiderich* [2010] attributed the late Miocene Mg/Ca_{bf} increase present in Atlantic records in part to increased $\Delta[CO_3^{=}]$ due to changes in circulation patterns, as reflected in increased carbonate preservation in the Atlantic at the expense of the Pacific. That hypothesis would lead to the expectation of reduced $\Delta[CO_3^{=}]$ reflected in Pacific records, which is the opposite of what our $\Delta[CO_3^{=}]$ reconstruction shows.

[56] Reconstructions from equations (7a) and (7b) both show an increase and subsequent decrease (for equation (7a)) in $\Delta[CO_3^{=}]$ during the middle Eocene that could be viewed as supporting evidence for a deepening of the CCD in this interval [*Tripati et al.*, 2005; *Lyle et al.*, 2006]. The high Paleocene $\Delta[CO_3^{=}]$, and decrease during the early Eocene, is consistent with the suggestion by *Hancock et al.* [2007] that the CCD was deep (>4000 m) for an interval of the late Paleocene–early Eocene, although the implied whole-ocean saturation with respect to $CaCO_3$ is extreme.

4.1.4. Summary

[57] The analysis above supports the conclusion that the Mg/Ca_{bf}, $\delta^{18}O_{bf}$, and NJSL records are easily reconcilable in the Oligocene–early Miocene. In this interval the records have potentially interesting implications for the evolution of ice sheets and ocean carbonate chemistry, but there is inadequate constraint on the Mg/Ca_{bf} sensitivity to temperature and Mg/Ca_{sw} to draw firm conclusions. Calculations based on equation (7a) broadly support our assumption of constant $\delta^{18}O_{ice}$ (although at a lower value) and CCD-based $\Delta[CO_3^{=}]$ changes for the Oligocene–early Miocene; for the same interval, the calculations based on equation (7b) support the *Farkaš et al.* [2007] reconstruction of Mg/Ca_{sw}, but are at odds with the assumption of constant $\delta^{18}O_{ice}$ and the Pacific CCD reconstruction. Better constraint on the Mg/Ca_{bf} sensitivities would allow more robust conclusions; in the case of high Mg/Ca_{sw} sensitivity the first order (>10 Myr) variations could be reconciled with small changes in the Mg/Ca_{sw} model.

[58] The records in the middle–late Miocene are more difficult to reconcile. While a decrease in $\delta^{18}O_{ice}$ in conjunction with growth and stabilization of the East Antarctic ice sheet conforms to our expectation, the magnitude of the implied increase is larger than expected. If further research confirms the NJSL and Mg/Ca_{bf} trends in this interval, then reconciling this with $\delta^{18}O_{bf}$ most likely requires a combination of Mg/Ca_{sw}, $\delta^{18}O_{ice}$, and $\Delta[CO_3^{=}]$ variations.

[59] The Paleocene–Eocene records are not easily reconciled, requiring extreme variations in $\delta^{18}O_{ice}$, $\Delta[CO_3^{=}]$, or Mg/Ca_{sw}. The Paleocene records can only be reasonably explained by changing Mg/Ca_{sw}, assuming a high Mg/Ca_{bf} sensitivity; it is most likely that the Mg/Ca_{bf} record in this interval is inaccurate (see section 3.4). The discrepancy among records in the Eocene may be explainable by a combination of $\Delta[CO_3^{=}]$, $\delta^{18}O_{ice}$, and Mg/Ca_{sw} variations, but more robust records are needed to confirm the second-order (5–10 Myr) variations in Mg/Ca_{bf}. The discrepancy in this interval also highlights the anomalously high NJSL in the early–middle Eocene; we assume ice free conditions at warm intervals throughout the Paleocene–early Eocene, with growth and decay of temporary glaciers during cold intervals, but we cannot rule out the possibility of growth of permanent ice sheets in the Paleocene and middle Eocene.

[60] From these observations, we conclude that, while it is possible that $IV_{\delta-Mg/Ca}$ reconstructions are an accurate reflection of ice sheet history, it is more likely that the large ice volumes implied by these reconstructions are artifacts of the constant $\delta^{18}O_{ice}$ and simplistic $\Delta[CO_3^{=}]$ history imposed in our calculations. Intervals with negative $IV_{\delta-Mg/Ca}$ must reflect either these artifacts or incompatibility of the $\delta^{18}O_{bf}$ and Mg/Ca_{bf} records. The same conclusion is not warranted for the $T_{Mg/Ca}$ reconstructions: these could be reconciled with reasonable ice volumes by assuming variable $\delta^{18}O_{ice}$. In the case of $T_{\delta-SL}$ and IV_{SL}, any artifacts from assuming constant $\delta^{18}O_{ice}$ are reflected in the temperature rather than ice volume reconstruction.

[61] The lack of sea level records comparable with NJSL and continuous through the late Miocene–Pleistocene (<9 Ma) means that we are only able to calculate $IV_{\delta-Mg/Ca}$ in this interval, and we have concluded that these reconstructions are not reliable. *Miller et al.* [2005, 2011, also submitted manuscript, 2011] provide a sea level reconstruction for this interval based solely on $\delta^{18}O_{bf}$, constrained by well-founded assumptions about the relative contribution of temperature and ice volume in glacial-interglacial cycles and the magnitude and timing of cooling since the late Miocene. The resulting sea levels in the late Miocene are similar to NJSL [*Miller et al.*, 2005, 2011] and are consistent with well-constrained sea level records in the late Pliocene (Miller et al., submitted manuscript, 2011). We have calculated temperature based on this sea level reconstruction using equation (1), and refer to these records when relevant in the discussion below (Figures 9 and S7).

4.2. Cenozoic Changes in Temperature and Ice Volume

[62] The transition from the early Cenozoic greenhouse to the late Cenozoic icehouse climate has long been inferred from $\delta^{18}O_{bf}$ records as a gradual cooling through the Eocene followed by three steps: the Eocene/Oligocene transition, middle Miocene, and Plio–Pleistocene [e.g., *Shackleton and Kennett*, 1975; *Miller et al.*, 1987; *Zachos et al.*, 2001; *Cramer et al.*, 2009] (see Figure 1). The default assumption has been that each of these steps represents a combination of temperature and ice-volume changes [e.g., *Crowley and Kim*, 1995; *Zachos et al.*, 2001; *Hansen et al.*, 2008]. That view has received some support from models involving ice

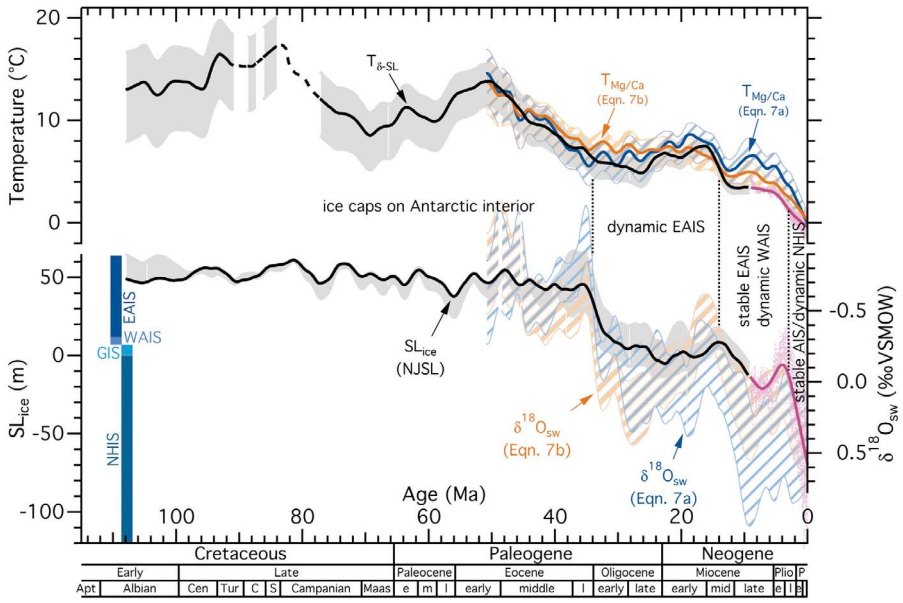

Figure 9. Summary of temperature and ice volume reconstructions since the Early Cretaceous, based on those in Figure 6 but smoothed to show only variations on >5 Myr timescales. As in Figure 6, the reconstructions based on NJSL and $\delta^{18}O_{bf}$ ($T_{\delta-SL}$ and IV_{SL}) are shown in black while reconstructions based on Mg/Ca_{bf} and $\delta^{18}O_{bf}$ ($T_{Mg/Ca}$ and $IV_{\delta-Mg/Ca}$) are shown in blue (equation (7a)) and orange (equation (7b)). We have added the late Miocene–Pleistocene sea level and temperature reconstruction based on scaling the $\delta^{18}O_{bf}$ record from *Miller et al.* [2011] (see Figure S7). Note that the cloud of points are individual estimates from scaled $\delta^{18}O_{bf}$ and are not equivalent to the confidence bands surrounding the other smooth curves. Styles of large ice sheet behavior through the Cenozoic are shown for comparison [after *Bertler and Barrett*, 2010]; vertical blue bars indicate the approximate cumulative range of sea level variations due to ice sheets (EAIS = east Antarctic ice sheet, WAIS = west Antarctic ice sheet, GIS = Greenland ice sheet, NHIS = northern hemisphere ice sheets). In Figure 9 (bottom) we emphasize the SL_{ice} from NJSL as our most reasonable ice volume reconstruction, but we plot the uncertainty bands for the $\delta^{18}O$-Mg/Ca reconstructions to acknowledge the uncertainty in $\delta^{18}O_{sw}$ reconstructions, although these do not necessarily reflect realistic uncertainty in ice volume (see Figure 8). A version of Figure 9 with the "best choice" $IV_{\delta-Mg/Ca}$ results plotted is available as Figure S9. Reconstructions shown in Figures 9 and S9 are available as tabulated data in the auxiliary material.

sheet dynamics [*Oerlemans*, 2004], but can be questioned in light of models indicating strong threshold effects in the growth of continent-scale ice sheets [*DeConto and Pollard*, 2003]. We consider as an appropriate null hypothesis that on >5 Myr timescales temperatures change only gradually, but ice sheets may respond abruptly to climate thresholds. The expectation that long-term temperature should change only gradually is based on an assumption that changes in the equilibrium atmospheric pCO_2 drive global temperature changes over these timescales [e.g., *Royer et al.*, 2004] and recognition that the balance between addition of CO_2 through volcanic and tectonic processes and removal of CO_2 by weathering sets the equilibrium pCO_2 level [e.g., *Walker et al.*, 1981; *Toggweiler*, 2008]. If the weathering sensitivity to atmospheric pCO_2 also responds primarily to tectonic processes, such as mountain building and the latitudinal distribution of continents, then the rate of change in pCO_2 is limited to slow tectonic rates. Our analysis is consistent with this null hypothesis, though still with considerable uncertainty.

[63] We find that the second-order (~10 Myr timescale; e.g., Figure 9) features of the Cenozoic cooling of the deep ocean and growth of continental ice volume are largely uncorrelated. Statistical analysis of variability in the ice volume and temperature reconstructions confirms our qualitative observations: the correlation between ice volume and temperature variability at 2–22 Myr timescales is not in general significantly different from the expectation for uncorrelated random processes (Figure S6). Qualitatively, we find that ice sheets remained small as deep-ocean temperatures cooled through the Eocene, while the large, abrupt increase in ice volume near the Eocene/Oligocene boundary occurred when cooling either slowed (according to $T_{\delta-SL}$) or ceased ($T_{Mg/Ca}$; Figures 6, 9, and S8). Importantly, both $T_{\delta-SL}$ and $T_{Mg/Ca}$ indicate that deep ocean temperatures during the early Miocene were equivalent to those during the late Eocene, although ice volume was significantly different. Cooling during the middle Miocene was accompanied by some increase in ice volume, but ice growth continued with temperatures stable or warming in the late Miocene (Figures 6, 9, and S7).

[64] The relationship between cooling and ice sheet growth in the late Miocene–Pleistocene is not clear from our analysis. Increasing amplitude of glacial-interglacial cycles in $\delta^{18}O_{bf}$ records in the late Pliocene (2.5–2.8 Ma) and Pleistocene (0.6–1.1 Ma) requires increasing northern hemisphere ice volume during glacial periods, implying

increases in the long term mean ice volume. Our $T_{Mg/Ca}$ reconstructions show overall cooling from the late Miocene–Pleistocene (<8 Ma) with an early Pliocene inflection to more rapid cooling (<4.5 Ma; Figures 6 and S7). We hesitate to interpret higher frequency variability (see Figures S5 and S6), but there is no obvious change in cooling rate associated with the late Pliocene and Pleistocene increases in glacial-interglacial amplitude, resulting in increases in $IV_{\delta-Mg/Ca}$ at these times. Miller et al. (submitted manuscript, 2011) assumed that cooling occurred mainly in a ~2 Myr interval prior to the late Pliocene increase in glacial-interglacial amplitude; this results in temperature and ice volume trends similar to our $T_{Mg/Ca}$ and $IV_{\delta-Mg/Ca}$ results, but beginning at lower temperature and ice volume consistent with our late Miocene $T_{\delta-SL}$ and IV_{SL} results (Figures 9, S7, and S9). These three reconstructions agree in showing early Pliocene cooling associated with ice volume decrease, with no obvious change in rate of cooling associated with late Pliocene–early Pleistocene ice volume increase.

[65] It is worth noting the caveat that deep ocean temperature variations may be decoupled from surface temperatures, although it is common to use the oversimplification that deep ocean temperature changes reflect (latitudinally consistent) high-latitude surface temperatures [e.g., *Zachos et al.*, 2001; *Cramer et al.*, 2009] and have also been used as a proxy for mean surface temperatures [e.g., *Crowley and Kim*, 1995; *Hansen et al.*, 2008]. Deep ocean temperatures reflect the surface/intermediate ocean temperatures at deep-water source regions, and the relative strengths and latitudinal position of those source regions should be expected to vary through time. The homogeneity of $\delta^{18}O_{bf}$ from different ocean basins during the Eocene implies that there was little differentiation with respect to temperature among deep water source regions [*Cramer et al.*, 2009]. This contrasts with large $\delta^{18}O_{bf}$ gradients between ocean basins beginning in the Oligocene [*Cramer et al.*, 2009] and the ~2°C difference between NADW and AABW in the modern ocean. The differentiation between temperatures in Northern and Southern Hemisphere deep-water source regions is primarily the result of the development of the Antarctic circumpolar current [*Toggweiler and Samuels*, 1995; *Toggweiler and Bjornsson*, 2000; *Cramer et al.*, 2009]. This resulted in a physical separation of the Southern Hemisphere deep water source regions around Antarctica from warmer midlatitude surface waters, a net transport of heat from the Southern to the Northern Hemisphere, and increased deep water production in the Northern Hemisphere. Under at least one model parameterization, the net result is a warming in most of the deep ocean (compare Figures 3–6 in the work by *Toggweiler and Bjornsson* [2000]), concomitant with cooling and thermal isolation of Antarctica that favors ice sheet growth. In addition, changes in the depth of the sills around Iceland have been implicated in changes in the strength of deep water production in the North Atlantic during the Neogene [*Wright and Miller*, 1996; *Poore et al.*, 2006] and in the early Oligocene [*Abelson et al.*, 2008] With a shallow sill, any deep water production would presumably be sourced from warmer surface waters south of Iceland, whereas a deep sill would allow deep water formation at colder, more northern latitudes.

[66] We therefore cannot rule out an abrupt shift to cooler mean surface temperatures coincident with the abrupt shift to larger ice volume in the earliest Oligocene. It is plausible that the lack of such a cooling in our reconstructions reflects a decoupling of deep ocean and mean surface temperatures at this time, or that a cooling of mean deep ocean temperatures is not reflected in our reconstructions. *Cramer et al.* [2009] showed that a ~0.5‰ difference in $\delta^{18}O_{bf}$ between the Southern Ocean and Pacific developed near the Eocene/Oligocene boundary, in conjunction with the large increase in ice volume shown here. If we assume that difference is entirely due to temperature, then an abrupt but persistent ~2°C cooling occurred in the Southern Ocean coincident with the abrupt and persistent increase in ice volume. The lack of a significant increase in the rate of cooling at this time in the Pacific $T_{\delta-SL}$ reconstruction may be due to increased influence of warmer North Atlantic sourced deep water and lesser influence of colder Southern Ocean sourced deep water, or it may reflect lack of cooling in a possible North Pacific deep water source region. It is also possible that the different $\delta^{18}O_{bf}$ trends at this time reflect different variations in local (non-ice volume) $\delta^{18}O_{sw}$ rather than temperature; large variations in $\delta^{18}O_{sw}$ in the Atlantic basins could be offset by much smaller $\delta^{18}O_{sw}$ changes in the Pacific due to its much larger volume. It should be noted that in the modern ocean $\delta^{18}O_{bf}$ is a poor indicator of deep ocean inhomogeneity with respect to temperature and $\delta^{18}O_{sw}$ because the $\delta^{18}O_{sw}$ difference between AABW and NADW is largely offset by the temperature difference when incorporated into $\delta^{18}O_{bf}$. There is evidence that the earliest Oligocene glaciation was accompanied by a sharp decrease in surface temperature [*Lear et al.*, 2008; *Katz et al.*, 2008; *Eldrett et al.*, 2009; *Liu et al.*, 2009] and decrease in pCO_2 [*Pearson et al.*, 2009], although it is not clear that this decrease entails a permanent shift to cooler temperatures rather than a temporary perturbation.

5. Conclusions

[67] We have demonstrated that available $\delta^{18}O_{bf}$, Mg/Ca_{bf} and sea level curves are reconcilable under reasonable assumptions. Mg/Ca_{bf} can be used to constrain temperature, and combined with $\delta^{18}O_{bf}$ to constrain ice volume (Figure 5); sea level can be used to constrain ice volume (Figure 3), and combined with $\delta^{18}O_{bf}$ to constrain temperature (Figure 4). The resulting records of temperature and ice volume are largely independently constructed, other than sharing the requirement of ice-free conditions in the early–middle Eocene. Most importantly, the temporal pattern of temperature change and ice volume increase from Eocene to Miocene times is mutually consistent between the two approaches (Figures 6, 9, and S5). The reconstructions of these second-order patterns are fully independent, and the coherence of the independent records can be used as evidence for the use of these parameters as robust climate proxies.

[68] We have identified a complementarity between the assumed Mg/Ca_{bf} sensitivities to temperature and Mg/Ca_{sw}. In the context of Cenozoic climate and Mg/Ca_{sw} changes we demonstrate that Mg/Ca_{bf} must either have high sensitivity to both temperature and Mg/Ca_{sw} or low sensitivity to both (Figure 7). This provides a framework for interpreting the Cenozoic Mg/Ca_{bf} record, but a robust calibration is needed for Mg/Ca_{bf} offsets between species analyzed from the

geologic record and species used for temperature calibrations. The calibration of these species offsets is more complicated for Mg/Ca_{bf} than for $\delta^{18}O_{bf}$, because of the possibility that different species have different sensitivities to Mg/Ca_{sw} and $\Delta[CO_3^{=}]$. We believe that our analysis indicates this problem is surmountable, and that the calibration of species offsets will allow use of Mg/Ca_{bf} as a robust climate proxy.

[69] Our calculations challenge the commonly used assumption that ice volume and temperature are proportionally represented throughout the late Cenozoic $\delta^{18}O_{bf}$ record. Instead, our results indicate that the correlation of temperature decrease and ice volume increase is not significantly different from random (Figure S6). Qualitatively, the Cenozoic increase in ice volume occurred primarily in two steps, in the earliest Oligocene and near the middle/late Miocene boundary, whereas the Cenozoic deep ocean cooling occurred in two prolonged intervals: the middle–late Eocene and the late Miocene–Pleistocene (Figures 6 and 9). The more detailed evolution of temperature and ice volume through the Cenozoic would be subject to greater uncertainty due to inadequate constraint on Mg/Ca_{bf} and sea level and the parameters needed to interpret these records. Despite these shortcomings, our analysis provides the best available synthesis of long-term temperature and ice-volume changes since the Late Cretaceous.

Notation

$\delta^{18}O_{bf}$	benthic foraminiferal $\delta^{18}O$ relative to VPDB standard (‰).
$\delta^{18}O_{sw}$	seawater $\delta^{18}O$, relative to VSMOW (‰).
$\delta^{18}O_{ice}$	$\delta^{18}O$ of continental ice sheets, relative to VSMOW (‰).
NJSL	sea level as measured using cores from the New Jersey coastal plain (m).
SL_{ice}	change in sea level due to growth and decay of continental ice sheets (m).
SL_{basin}	sea level contribution from variations in the volume of the ocean basins (m).
k	change in $\delta^{18}O_{sw}$ per unit change in SL_{ice}; see equation (9) (‰/m).
Mg/Ca_{bf}	benthic foraminiferal Mg/Ca ratio (mmol/mol).
Mg/Ca_{sw}	seawater Mg/Ca ratio (mol/mol).
Mg/Ca_{corr}	Mg/Ca_{bf} corrected for variations in $\Delta[CO_3^{=}]$ and Mg/Ca_{sw} (mmol/mol).
H	partition exponent for Mg/Ca_{sw} in Mg/Ca_{bf} see equation (2) (unitless).
$\Delta[CO_3^{=}]$	carbonate ion saturation state for $CaCO_3$ ($[CO_3^{=}]_{seawater} - [CO_3^{=}]_{saturation}$) ($\mu$mol/mol).
CCD	calcite compensation depth; $CaCO_3$-rich to $CaCO_3$-poor sediment boundary (km).
$T_{Mg/Ca}$	ocean temperature calculated from Mg/Ca_{bf} (°C).
$T_{\delta-SL}$	ocean temperature calculated from $\delta^{18}O_{bf}$ using SL_{ice} to constrain $\delta^{18}O_{sw}$ (°C).
$IV_{\delta-Mg/Ca}$	ice volume calculated from $\delta^{18}O_{bf}$ using Mg/Ca_{bf} to constrain temperature (%).
IV_{SL}	ice volume calculated from SL_{ice} (%).

[70] **Acknowledgments.** We are very grateful to two anonymous reviewers, whose comments led to major changes in our analysis and forced us to deal with the full complexity of the Mg/Ca_{bf} proxy. This research was funded in part by NSF grant OCE-0927663 to B.S. Cramer.

References

Abelson, M., A. Agnon, and A. Almogi-Labin (2008), Indications for control of the Iceland plume on the Eocene–Oligocene "greenhouse-icehouse" climate transition, *Earth Planet. Sci. Lett.*, *265*(1–2), 33–48, doi:10.1016/j.epsl.2007.09.021.

Bamber, J. L., R. L. Layberry, and S. P. Gogineni (2001), A new ice thickness and bed data set for the Greenland ice sheet: 1. Measurement, data reduction, and errors, *J. Geophys. Res.*, *106*(D24), 33,773–33,780, doi:10.1029/2001JD900054.

Barrett, P. J. (Ed.) (1989), Antarctic Cenozoic history from the CIROS-1 drillhole, McMurdo Sound, *Bull. 245*, 254 pp., Dep. of Sci. and Ind. Res., Wellington, New Zealand.

Barrett, P. (1999), Antarctic climate history over the last 100 million years, *Terra Antarct. Rep.*, *3*, 53–72.

Barrett, P. J. (2007), Cenozoic climate and sea level history from glacimarine strata off the Victoria Land Coast, Cape Roberts Project, Antarctica, in *Glacial Processes and Products*, edited by M. J. Hambrey et al., *Spec. Publ. Int. Assoc. Sedimentol.*, *39*, 259–287, doi:10.1002/9781444304435.ch15.

Bemis, B. E., H. J. Spero, J. Bijma, and D. W. Lea (1998), Reevaluation of the oxygen isotopic composition of planktonic foraminifera: Experimental results and revised paleotemperature equations, *Paleoceanography*, *13*(2), 150–160, doi:10.1029/98PA00070.

Berger, W. H., and U. von Rad (1972), Cretaceous and Cenozoic sediments from the Atlantic Ocean, *Initial Rep. Deep Sea Drill. Proj.*, *14*, 787–954, doi:10.2973/dsdp.proc.14.127.1972.

Bertler, N. A. N., and P. J. Barrett (2010), Vanishing polar ice sheets, in *Changing Climates, Earth Systems and Society*, edited by J. Dodson, pp. 49–83, Springer, Dordrecht, Netherlands, doi:10.1007/978-90-481-8716-4_4.

Billups, K., and K. Scheiderich (2010), A synthesis of Late Oligocene through Miocene deep sea temperatures as inferred from foraminiferal Mg/Ca ratios, in *Carbonate Systems During the Oligocene–Miocene Climatic Transition*, edited by C. B. M. Mutti and W. E. Piller, *Spec. Publ. Int. Assoc. Sedimentol.*, *42*, 1–16.

Billups, K., and D. P. Schrag (2002), Paleotemperatures and ice volume of the past 27 Myr revisited with paired Mg/Ca and $^{18}O/^{16}O$ measurements on benthic foraminifera, *Paleoceanography*, *17*(1), 1003, doi:10.1029/2000PA000567.

Billups, K., and D. P. Schrag (2003), Application of benthic foraminiferal Mg/Ca ratios to questions of Cenozoic climate change, *Earth Planet. Sci. Lett.*, *209*, 181–195, doi:10.1016/S0012-821X(03)00067-0.

Browning, J. V., K. G. Miller, and D. K. Pak (1996), Global implications of lower to middle Eocene sequence boundaries on the New Jersey coastal plain: The icehouse cometh, *Geology*, *24*, 639–642, doi:10.1130/0091-7613(1996)024<0639:GIOLTM>2.3.CO;2.

Bryan, S. P., and T. M. Marchitto (2008), Mg/Ca–temperature proxy in benthic foraminifera: New calibrations from the Florida Straits and a hypothesis regarding Mg/Li, *Paleoceanography*, *23*, PA2220, doi:10.1029/2007PA001553.

Cande, S. C., and D. V. Kent (1992), A new geomagnetic polarity time scale for the Late Cretaceous and Cenozoic, *J. Geophys. Res.*, *97*(B10), 13,917–13,951, doi:10.1029/92JB01202.

Cande, S. C., and D. V. Kent (1995), Revised calibration of the geomagnetic polarity timescale for the Late Cretaceous and Cenozoic, *J. Geophys. Res.*, *100*, 6093–6095, doi:10.1029/94JB03098.

Charette, M. A., and W. H. F. Smith (2010), The volume of Earth's ocean, *Oceanography*, *23*(2), 112–114, doi:10.5670/oceanog.2010.51.

Cleveland, W. S. (1979), Robust locally weighted regression and smoothing scatterplots, *J. Am. Stat. Assoc.*, *74*(368), 829–836, doi:10.2307/2286407.

Coggon, R. M., D. A. H. Teagle, C. E. Smith-Duque, J. C. Alt, and M. J. Cooper (2010), Reconstructing past seawater Mg/Ca and Sr/Ca from mid-ocean ridge flank calcium carbonate veins, *Science*, *327*(5969), 1114–1117, doi:10.1126/science.1182252.

Cogné, J.-P., and E. Humler (2006), Trends and rhythms in global seafloor generation rate, *Geochem. Geophys. Geosyst.*, *7*, Q03011, doi:10.1029/2005GC001148.

Cogné, J.-P., E. Humler, and V. Courtillot (2006), Mean age of oceanic lithosphere drives eustatic sea-level change since Pangea breakup, *Earth Planet. Sci. Lett.*, *245*(1–2), 115–122, doi:10.1016/j.epsl.2006.03.020.

Conrad, C. P., and C. Lithgow-Bertelloni (2007), Faster seafloor spreading and lithosphere production during the mid-Cenozoic, *Geology*, *35*(1), 29–32, doi:10.1130/G22759A.1.

Costa, K. B., F. A. L. Toledo, M. A. G. Pivel, C. A. V. Moura, and F. Chemale Jr. (2006), Evaluation of two genera of benthic foraminifera for down-core paleotemperature studies in the western South Atlantic, *Braz. J. Oceanogr.*, *54*, 75–84, doi:10.1590/S1679-87592006000100007.

Coxall, H. K., P. A. Wilson, H. Pälike, C. H. Lear, and J. Backman (2005), Rapid stepwise onset of Antarctic glaciation and deeper calcite

compensation in the Pacific Ocean, *Nature*, *433*, 53–57, doi:10.1038/nature03135.

Cramer, B. S., J. R. Toggweiler, J. D. Wright, M. E. Katz, and K. G. Miller (2009), Ocean overturning since the Late Cretaceous: Inferences from a new benthic foraminiferal isotope compilation, *Paleoceanography*, *24*, PA4216, doi:10.1029/2008PA001683.

Crowley, T. J., and K.-Y. Kim (1995), Comparison of longterm greenhouse projections with the geologic record, *Geophys. Res. Lett.*, *22*(8), 933–936, doi:10.1029/95GL00799.

Curry, W. B., and T. M. Marchitto (2008), A secondary ionization mass spectrometry calibration of Cibicidoides pachyderma Mg/Ca with temperature, *Geochem. Geophys. Geosyst.*, *9*, Q04009, doi:10.1029/2007GC001620.

Dawber, C. F., and A. K. Tripati (2011), Constraints on glaciation in the middle Eocene (46–37 ma) from Ocean Drilling Program (ODP) Site 1209 in the tropical Pacific Ocean, *Paleoceanography*, *26*, PA2208, doi:10.1029/2010PA002037.

DeConto, R. M., and D. Pollard (2003), Rapid Cenozoic glaciation of Antarctica induced by declining atmospheric CO_2, *Nature*, *421*, 245–249, doi:10.1038/nature01290.

Delaney, M. L., A. W. H. Bé, and E. A. Boyle (1985), Li, Sr, Mg, and Na in foraminiferal calcite shells from laboratory culture, sediment traps, and sediment cores, *Geochim. Cosmochim. Acta*, *49*(6), 1327–1341, doi:10.1016/0016-7037(85)90284-4.

Demicco, R. V. (2004), Modeling seafloor-spreading rates through time, *Geology*, *32*(6), 485–488, doi:10.1130/G20409.1.

Demicco, R. V., T. K. Lowenstein, L. A. Hardie, and R. J. Spencer (2005), Model of seawater composition for the Phanerozoic, *Geology*, *33*(11), 877–880, doi:10.1130/G21945.1.

Dickson, J. A. D. (2002), Fossil echinoderms as monitor of the Mg/Ca ratio of Phanerozoic oceans, *Science*, *298*(5596), 1222–1224, doi:10.1126/science.1075882.

Dickson, J. A. D. (2004), Echinoderm skeletal preservation: Calcite-aragonite seas and the Mg/Ca ratio of Phanerozoic oceans, *J. Sediment. Res.*, *74*(3), 355–365, doi:10.1306/112203740355.

Dutton, A., K. C. Lohmann, and R. M. Leckie (2004), Insights from the Paleogene tropical Pacific: Foraminiferal stable isotope and elemental results from Site 1209, Shatsky Rise, *Paleoceanography*, *20*, PA3004, doi:10.1029/2004PA001098.

Dutton, A., K. Lohmann, and R. Leckie (2005), Data report: Stable isotope and Mg/Ca of Paleocene and Eocene foraminifers, ODP Site 1209, Shatsky Rise, *Proc. Ocean Drill. Program Sci. Results*, *198*, 1–15, doi:10.2973/odp.proc.sr.198.119.2005.

Elderfield, H., J. Yu, P. Anand, T. Kiefer, and B. Nyland (2006), Calibrations for benthic foraminiferal Mg/Ca paleothermometry and the carbonate ion hypothesis, *Earth Planet. Sci. Lett.*, *250*(3–4), 633–649, doi:10.1016/j.epsl.2006.07.041.

Eldrett, J. S., D. R. Greenwood, I. C. Harding, and M. Huber (2009), Increased seasonality through the Eocene to Oligocene transition in northern high latitudes, *Nature*, *459*(7249), 969–973, doi:10.1038/nature08069.

Emiliani, C. (1954), Temperatures of Pacific bottom waters and polar superficial waters during the Tertiary, *Science*, *119*(3103), 853–855, doi:10.1126/science.119.3103.853.

Emiliani, C. (1961), The temperature decrease of surface sea-water in high latitudes and of abyssal-hadal water in open oceanic basins during the past 75 million years, *Deep Sea Res.*, *8*(2), 144–147, doi:10.1016/0146-6313(61)90006-5.

Expedition 313 Scientists (2010), New Jersey Shallow Shelf: Shallow-water drilling of the New Jersey continental shelf: Global sea level and architecture of passive margin sediments [online], *Integr. Ocean Drill. Program Prelim. Rep.*, *313*, 82 pp., doi:10.2204/iodp.pr.313.2010. [Available at http://publications.iodp.org/preliminary_report/313/]

Fairbanks, R. G. (1989), A 17,000-year glacio-eustatic sea level record: Influence of glacial melting rates on the Younger Dryas event and deep-ocean circulation, *Nature*, *342*, 637–642, doi:10.1038/342637a0.

Fairbanks, R. G., and R. K. Matthews (1978), The marine oxygen isotope record in Pleistocene coral, Barbados, West Indies, *Quat. Res.*, *10*(2), 181–196, doi:10.1016/0033-5894(78)90100-X.

Farkaš, J., F. Böhm, K. Wallmann, J. Blenkinsop, A. Eisenhauer, R. van Geldern, A. Munnecke, S. Voigt, and J. Veizer (2007), Calcium isotope record of Phanerozoic oceans: Implications for chemical evolution of seawater and its causative mechanisms, *Geochim. Cosmochim. Acta*, *71*(21), 5117–5134, doi:10.1016/j.gca.2007.09.004.

Filipsson, H. L., J. M. Bernhard, S. A. Lincoln, and D. C. McCorkle (2010), A culture-based calibration of benthic foraminiferal paleotemperature proxies: δ^{18}O and Mg/Ca results, *Biogeosciences*, *7*(4), 1335–1347, doi:10.5194/bg-7-1335-2010.

Fontanier, C., A. Mackensen, F. J. Jorissen, P. Anschutz, L. Licari, and C. Griveaud (2006), Stable oxygen and carbon isotopes of live benthic foraminifera from the Bay of Biscay: Microhabitat impact and seasonal variability, *Mar. Micropaleontol.*, *58*(3), 159–183, doi:10.1016/j.marmicro.2005.09.004.

Gaffin, S. (1987), Ridge volume dependence on seafloor generation rate and inversion using long term sealevel change, *Am. J. Sci.*, *287*(6), 596–611, doi:10.2475/ajs.287.6.596.

Gradstein, F. M., J. G. Ogg, and A. G. Smith (Eds.) (2004), *A Geologic Time Scale 2004*, Cambridge Univ. Press, Cambridge, U. K., doi:10.2277/0511074050.

Hambrey, M. J., B. Larsen, and W. U. Ehrmann (1991), The glacial record from the Prydz Bay continental shelf, east Antarctica, *Proc. Ocean Drill. Program Sci. Results*, *119*, 77–132, doi:10.2973/odp.proc.sr.119.1991.

Hancock, H., G. Dickens, E. Thomas, and K. Blake (2007), Reappraisal of early Paleogene CCD curves: Foraminiferal assemblages and stable carbon isotopes across the carbonate facies of Perth Abyssal Plain, *Int. J. Earth Sci.*, *96*(5), 925–946, doi:10.1007/s00531-006-0144-0.

Hansen, J., M. Sato, P. Kharecha, D. Beerling, R. Berner, V. Masson-Delmotte, M. Pagani, M. Raymo, D. L. Royer, and J. C. Zachos (2008), Target atmospheric CO_2: Where should humanity aim?, *Open Atmos. Sci. J.*, *2*, 217–231, doi:10.2174/1874282300802010217.

Haq, B. U., J. Hardenbol, and P. R. Vail (1987), Chronology of fluctuating sea levels since the Triassic, *Science*, *235*(4793), 1156–1167, doi:10.1126/science.235.4793.1156.

Hardie, L. A. (1996), Secular variation in seawater chemistry: An explanation for the coupled secular variation in the mineralogies of marine limestones and potash evaporites over the past 600 m.y., *Geology*, *24*(3), 279–283, doi:10.1130/0091-7613(1996)024<0279:SVISCA>2.3.CO;2.

Hasiuk, F. J., and K. C. Lohmann (2010), Application of calcite Mg partitioning functions to the reconstruction of paleocean Mg/Ca, *Geochim. Cosmochim. Acta*, *74*(23), 6751–6763, doi:10.1016/j.gca.2010.07.030.

Healey, S. L., R. C. Thunell, and B. H. Corliss (2008), The Mg/Ca-temperature relationship of benthic foraminiferal calcite: New core-top calibrations in the C temperature range, *Earth Planet. Sci. Lett.*, *272*(3–4), 523–530, doi:10.1016/j.epsl.2008.05.023.

Horita, J., H. Zimmermann, and H. D. Holland (2002), Chemical evolution of seawater during the Phanerozoic: Implications from the record of marine evaporites, *Geochim. Cosmochim. Acta*, *66*(21), 3733–3756, doi:10.1016/S0016-7037(01)00884-5.

Huber, M. (2008), Climate change: A hotter greenhouse?, *Science*, *321*(5887), 353–354, doi:10.1126/science.1161170.

Hut, G. (1987), *Consultants' Group Meeting on Stable Isotope Reference Samples for Geochemical and Hydrological Investigations, Vienna, 16–18 September 1985, Report to the Director General*, Int. At. Energy Agency, Vienna.

Jaffrés, J. B. D., G. A. Shields, and K. Wallmann (2007), The oxygen isotope evolution of seawater: A critical review of a long-standing controversy and an improved geological water cycle model for the past 3.4 billion years, *Earth Sci. Rev.*, *83*(1–2), 83–122, doi:10.1016/j.earscirev.2007.04.002.

John, C. M., G. D. Karner, and M. Mutti (2004), δ^{18}O and Marion Plateau backstripping: Combining two approaches to constrain late middle Miocene eustatic amplitude, *Geology*, *32*(9), 829–832, doi:10.1130/G20580.1.

John, C. M., G. D. Karner, E. Browning, R. M. Leckie, Z. Mateo, B. Carson, and C. Lowery (2011), Timing and magnitude of Miocene eustasy derived from the mixed siliciclastic-carbonate stratigraphic record of the northeastern Australian margin, *Earth Planet. Sci. Lett.*, *304*(3–4), 455–467, doi:10.1016/j.epsl.2011.02.013.

Katz, M. E., K. G. Miller, J. D. Wright, B. S. Wade, J. V. Browning, B. S. Cramer, and Y. Rosenthal (2008), Stepwise transition from the Eocene greenhouse to the Oligocene icehouse, *Nat. Geosci.*, *1*, 329–334, doi:10.1038/ngeo179.

Katz, M. E., B. S. Cramer, A. Franzese, B. Honisch, K. G. Miller, Y. Rosenthal, and J. D. Wright (2010), Traditional and emerging geochemical proxies in foraminifera, *J. Foraminiferal Res.*, *40*(2), 165–192, doi:10.2113/gsjfr.40.2.165.

Kim, S.-T., and J. R. O'Neil (1997), Equilibrium and nonequilibrium oxygen isotope effects in synthetic carbonates, *Geochim. Cosmochim. Acta*, *61*(16), 3461–3475, doi:10.1016/S0016-7037(97)00169-5.

Kominz, M. A., J. V. Browning, K. G. Miller, P. J. Sugarman, S. Mizintseva, and C. R. Scotese (2008), Late Cretaceous to Miocene sea-level estimates from the New Jersey and Delaware coastal plain coreholes: An error analysis, *Basin Res.*, *20*(2), 211–226, doi:10.1111/j.1365-2117.2008.00354.x.

Lear, C. H., H. Elderfield, and P. A. Wilson (2000), Cenozoic deep-sea temperatures and global ice volumes from Mg/Ca in benthic foraminiferal calcite, *Science*, *287*, 269–272, doi:10.1126/science.287.5451.269.

Lear, C. H., Y. Rosenthal, and N. Slowey (2002), Benthic foraminiferal Mg/Ca-paleothermometry: A revised core-top calibration, *Geochim.*

Cosmochim. Acta, *66*(19), 3375–3387, doi:10.1016/S0016-7037(02)00941-9.

Lear, C. H., Y. Rosenthal, and J. D. Wright (2003), The closing of a seaway: Ocean water masses and global climate change, *Earth Planet. Sci. Lett.*, *210*, 425–436, doi:10.1016/S0012-821X(03)00164-X.

Lear, C. H., Y. Rosenthal, H. K. Coxall, and P. A. Wilson (2004), Late Eocene to early Miocene ice sheet dynamics and the global carbon cycle, *Paleoceanography*, *19*, PA4015, doi:10.1029/2004PA001039.

Lear, C. H., T. R. Bailey, P. N. Pearson, H. K. Coxall, and Y. Rosenthal (2008), Cooling and ice growth across the Eocene–Oligocene transition, *Geology*, *36*(3), 251–254, doi:10.1130/G24584A.1.

Lear, C. H., E. M. Mawbey, and Y. Rosenthal (2010), Cenozoic benthic foraminiferal Mg/Ca and Li/Ca records: Toward unlocking temperatures and saturation states, *Paleoceanography*, *25*, PA4215, doi:10.1029/2009PA001880.

Lemke, P., et al. (2007), Observations: Changes in snow, ice and frozen ground, in *Climate Change 2007: The Physical Science Basis—Summary for Policymakers, Technical Summary and Frequently Asked Questions* chap. 4, pp. 337–383, Cambridge Univ. Press, Cambridge, U. K.

Lewis, A. R., D. R. Marchant, A. C. Ashworth, S. R. Hemming, and M. L. Machlus (2007), Major middle Miocene global climate change: Evidence from East Antarctica and the Transantarctic Mountains, *Geol. Soc. Am. Bull.*, *119*(11–12), 1449–1461, doi:10.1130/0016-7606(2007)119[1449:MMMGCC]2.0.CO;2.

Lewis, A. R., et al. (2008), Mid-Miocene cooling and the extinction of tundra in continental Antarctica, *Proc. Natl. Acad. Sci. U. S. A.*, *105*(31), 10,676–10,680, doi:10.1073/pnas.0802501105.

Lhomme, N., G. K. C. Clarke, and C. Ritz (2005), Global budget of water isotopes inferred from polar ice sheets, *Geophys. Res. Lett.*, *32*, L20502, doi:10.1029/2005GL023774.

Liu, Z., M. Pagani, D. Zinniker, R. DeConto, M. Huber, H. Brinkhuis, S. R. Shah, R. M. Leckie, and A. Pearson (2009), Global cooling during the Eocene–Oligocene climate transition, *Science*, *323*(5918), 1187–1190, doi:10.1126/science.1166368.

Lowenstein, T. K., M. N. Timofeeff, S. T. Brennan, L. A. Hardie, and R. V. Demicco (2001), Oscillations in Phanerozoic seawater chemistry: Evidence from fluid inclusions, *Science*, *294*(5544), 1086–1088, doi:10.1126/science.1064280.

Lyle, M., A. Olivarez Lyle, J. Backman, and A. Tripati (2006), Biogenic sedimentation in the Eocene equatorial Pacific—The stuttering greenhouse and Eocene carbonate compensation depth, *Proc. Ocean Drill. Program Sci. Results*, *199*, 1–35, doi:10.2973/odp.proc.sr.199.219.2005.

Lynch-Stieglitz, J., W. B. Curry, and N. Slowey (1999), A geostrophic transport estimate for the Florida Current from the oxygen isotope composition of benthic foraminifera, *Paleoceanography*, *14*(3), 360–373, doi:10.1029/1999PA900001.

Lythe, M. B., D. G. Vaughan, and the BEDMAP Consortium (2001), BEDMAP: A new ice thickness and subglacial topographic model of Antarctica, *J. Geophys. Res.*, *106*(B6), 11,335–11,351, doi:10.1029/2000JB900449.

Marchitto, T. M., S. P. Bryan, W. B. Curry, and D. C. McCorkle (2007), Mg/Ca temperature calibration for the benthic foraminifer Cibicidoides pachyderma, *Paleoceanography*, *22*, PA1203, doi:10.1029/2006PA001287.

Martin, P. A., D. W. Lea, Y. Rosenthal, N. J. Shackleton, M. Sarnthein, and T. Papenfuss (2002), Quaternary deep sea temperature histories derived from benthic foraminiferal Mg/Ca, *Earth Planet. Sci. Lett.*, *198*, 193–209, doi:10.1016/S0012-821X(02)00472-7.

Miller, K. G., R. G. Fairbanks, and G. S. Mountain (1987), Tertiary oxygen isotope synthesis, sea level history, and continental margin erosion, *Paleoceanography*, *2*(1), 1–19, doi:10.1029/PA002i001p00001.

Miller, K. G., G. S. Mountain, the Leg 150 Shipboard Party, and Members of the New Jersey Coastal Plain Drilling Project (1996), Drilling and dating New Jersey Oligocene–Miocene sequences: Ice volume, global sea level, and Exxon records, *Science*, *271*, 1092–1095, doi:10.1126/science.271.5252.1092.

Miller, K. G., G. S. Mountain, J. V. Browning, M. A. Kominz, P. J. Sugarman, N. Christie-Blick, M. E. Katz, and J. D. Wright (1998), Cenozoic global sea level, sequences, and the New Jersey Transect: Results from coastal plain and continental slope drilling, *Rev. Geophys.*, *36*(4), 569–601, doi:10.1029/98RG01624.

Miller, K. G., E. Barrera, R. K. Olsson, P. J. Sugarman, and S. M. Savin (1999), Does ice drive early Maastrichtian eustasy?, *Geology*, *27*, 783–786, doi:10.1130/0091-7613(1999)027<0783:DIDEME>2.3.CO;2.

Miller, K. G., P. J. Sugarman, J. V. Browning, M. A. Kominz, R. K. Olsson, M. D. Feigenson, and J. C. Hernández (2004), Upper Cretaceous sequences and sea-level history, New Jersey Coastal Plain, *Geol. Soc. Am. Bull.*, *116*(3), 368–393, doi:10.1130/B25279.1.

Miller, K. G., M. A. Kominz, J. V. Browning, J. D. Wright, G. S. Mountain, M. E. Katz, P. J. Sugarman, B. S. Cramer, N. Christie-Blick, and S. F. Pekar (2005), The Phanerozoic record of global sea-level change, *Science*, *310*(5752), 1293–1298, doi:10.1126/science.1116412.

Miller, K. G., J. D. Wright, M. E. Katz, J. V. Browning, B. S. Cramer, B. S. Wade, and S. F. Mizintseva (2008), A view of Antarctic ice-sheet evolution from sea-level and deep-sea isotope changes during the Late Cretaceous-Cenozoic, in *Antarctica: A Keystone in a Changing World: Proceedings of the 10th International Symposium on Antarctic Earth Sciences*, edited by A. K. Cooper et al., pp. 55–70, Natl. Acad. Press, Washington, D. C.

Miller, K. G., G. S. Mountain, J. D. Wright, and J. V. Browning (2011), A 180-million-year record of sea level and ice volume variations inferred from continental margin and deep-sea isotopic records, *Oceanography*, *24*(2), 40–53, doi:10.5670/oceanog.2011.26.

Müller, R. D., M. Sdrolias, C. Gaina, B. Steinberger, and C. Heine (2008), Long-term sea-level fluctuations driven by ocean basin dynamics, *Science*, *319*(5868), 1357–1362, doi:10.1126/science.1151540.

Naish, T. R., et al. (2001), Orbitally induced oscillations in the East Antarctic ice sheet at the Oligocene/Miocene boundary, *Nature*, *413*(6857), 719–723, doi:10.1038/35099534.

Oerlemans, J. (2004), Correcting the Cenozoic δ^{18}O deep-sea temperature record for Antarctic ice volume, *Palaeogeogr. Palaeoclimatol. Palaeoecol.*, *208*(3–4), 195–205, doi:10.1016/j.palaeo.2004.03.004.

Ogg, J. G., and A. G. Smith (2004), The geomagnetic polarity time scale, in *A Geologic Time Scale 2004*, edited by F. M. Gradstein, J. G. Ogg, and A. G. Smith, pp. 63–86, Cambridge Univ. Press, Cambridge, U. K., doi:10.2277/0511074050.

O'Neil, J. R., R. N. Clayton, and T. K. Mayeda (1969), Oxygen isotope fractionation in divalent metal carbonates, *J. Chem. Phys.*, *51*(12), 5547–5558, doi:10.1063/1.1671982.

Pearson, P. N., G. L. Foster, and B. S. Wade (2009), Atmospheric carbon dioxide through the Eocene-Oligocene climate transition, *Nature*, *461*, 1110–1113, doi:10.1038/nature08447.

Peck, V. L., J. Yu, S. Kender, and C. R. Riesselman (2010), Shifting ocean carbonate chemistry during the Eocene–Oligocene climate transition: Implications for deep-ocean Mg/Ca paleothermometry, *Paleoceanography*, *25*, PA4219, doi:10.1029/2009PA001906.

Pekar, S., and K. G. Miller (1996), New Jersey Oligocene "Icehouse" sequences (ODP Leg 150X) correlated with global δ^{18}O and Exxon eustatic records, *Geology*, *24*(6), 567–570, doi:10.1130/0091-7613(1996)024<0567:NJOISO>2.3.CO;2.

Pekar, S. F., N. Christie-Blick, M. A. Kominz, and K. G. Miller (2002), Calibration between eustatic estimates from backstripping and oxygen isotopic records for the Oligocene, *Geology*, *30*(10), 903–906, doi:10.1130/0091-7613(2002)030<0903:CBEEFB>2.0.CO;2.

Peltier, W. R. (1998), Postglacial variations in the level of the sea: Implications for climate dynamics and solid-earth geophysics, *Rev. Geophys.*, *36*, 603–689, doi:10.1029/98RG02638.

Peltier, W. R., and R. G. Fairbanks (2006), Global glacial ice volume and Last Glacial Maximum duration from an extended Barbados sea level record, *Quat. Sci. Rev.*, *25*(23–24), 3322–3337, doi:10.1016/j.quascirev.2006.04.010.

Poore, H. R., R. Samworth, N. J. White, S. M. Jones, and I. N. McCave (2006), Neogene overflow of Northern Component Water at the Greenland-Scotland Ridge, *Geochem. Geophys. Geosyst.*, *7*, Q06010, doi:10.1029/2005GC001085.

Pusz, A. E., R. C. Thunell, and K. G. Miller (2011), Deep water temperature, carbonate ion, and ice volume changes across the Eocene–Oligocene climate transition, *Paleoceanography*, *26*, PA2205, doi:10.1029/2010PA001950.

Raitzsch, M., H. Kuhnert, J. Groeneveld, and T. Bickert (2008), Benthic foraminifer Mg/Ca anomalies in South Atlantic core top sediments and their implications for paleothermometry, *Geochem. Geophys. Geosyst.*, *9*, Q05010, doi:10.1029/2007GC001788.

Rathmann, S., and H. Kuhnert (2008), Carbonate ion effect on Mg/Ca, Sr/Ca and stable isotopes on the benthic foraminifera Oridorsalis umbonatus off Namibia, *Mar. Micropaleontol.*, *66*(2), 120–133, doi:10.1016/j.marmicro.2007.08.001.

Rathmann, S., S. Hess, H. Kuhnert, and S. Mulitza (2004), Mg/Ca ratios of the benthic foraminifera Oridorsalis umbonatus obtained by laser ablation from core top sediments: Relationship to bottom water temperature, *Geochem. Geophys. Geosyst.*, *5*, Q12013, doi:10.1029/2004GC000808.

Raymo, M., J. X. Mitrovica, M. J. O'Leary, R. M. DeConto, and P. J. Hearty (2011), Departures from eustacy in Pliocene sea-level records, *Nat. Geosci.*, *4*, 328–332, doi:10.1038/ngeo1118.

Ries, J. B. (2004), Effect of ambient Mg/Ca ratio on Mg fractionation in calcareous marine invertebrates: A record of the oceanic Mg/Ca ratio over the Phanerozoic, *Geology*, *32*(11), 981–984, doi:10.1130/G20851.1.

Rosenthal, Y., E. A. Boyle, and N. C. Slowey (1997), Temperature control on the incorporation of Mg, Sr, F and Cd into benthic foraminiferal shells

from Little Bahama Bank: Prospects for thermocline paleoceanography, *Geochim. Cosmochim. Acta*, *61*, 3633–3643, doi:10.1016/S0016-7037(97)00181-6.

Rosenthal, Y., C. H. Lear, D. W. Oppo, and B. K. Linsley (2006), Temperature and carbonate ion effects on Mg/Ca and Sr/Ca ratios in benthic foraminifera: Aragonitic species Hoeglundina elegans, *Paleoceanography*, *21*, PA1007, doi:10.1029/2005PA001158.

Rowley, D. B. (2002), Rate of plate creation and destruction: 180 Ma to present, *Geol. Soc. Am. Bull.*, *114*(8), 927–933, doi:10.1130/0016-7606(2002)114<0927:ROPCAD>2.0.CO;2.

Rowley, D. B. (2008), Extrapolating oceanic age distributions: Lessons from the Pacific region, *J. Geol.*, *116*(6), 587–598, doi:10.1086/592276.

Royer, D. L., R. A. Berner, I. P. Montañez, N. J. Tabor, and D. J. Beerling (2004), CO_2 as a primary driver of Phanerozoic climate, *GSA Today*, *14*(3), 4–10, doi:10.1130/1052-5173(2004)014<4:CAAPDO>2.0.CO;2.

Savin, S. M. (1977), The history of the Earth's surface temperature during the past 100 million years, *Annu. Rev. Earth Planet. Sci.*, *5*(1), 319–355, doi:10.1146/annurev.ea.05.050177.001535.

Savin, S. M., R. G. Douglas, and F. G. Stehli (1975), Tertiary marine paleotemperatures, *Geol. Soc. Am. Bull.*, *86*(11), 1499–1510, doi:10.1130/0016-7606(1975)86<1499:TMP>2.0.CO;2.

Schrag, D. P., D. J. DePaolo, and F. M. Richter (1995), Reconstructing past sea surface temperatures: Correcting for diagenesis of bulk marine carbonate, *Geochim. Cosmochim. Acta*, *59*(11), 2265–2278, doi:10.1016/0016-7037(95)00105-9.

Segev, E., and J. Erez (2006), Effect of Mg/Ca ratio in seawater on shell composition in shallow benthic foraminifera, *Geochem. Geophys. Geosyst.*, *7*, Q02P09, doi:10.1029/2005GC000969.

Shackleton, N. J. (1974), Attainment of isotopic equilibrium between ocean water and the benthonic foraminifera genus Uvigerina: Isotopic changes in the ocean during the last glacial, *Colloq. Int. CNRS*, *219*, 203–209.

Shackleton, N. J., and J. P. Kennett (1975), Paleotemperature history of the Cenozoic and the initiation of Antarctic glaciation: Oxygen and carbon isotope analyses in DSDP Sites 277, 279, and 281, *Init. Rep. Deep Sea Drill. Proj.*, *29*, 743–755, doi:10.2973/dsdp.proc.29.117.1975.

Shevenell, A. E., J. P. Kennett, and D. W. Lea (2008), Middle Miocene ice sheet dynamics, deep-sea temperatures, and carbon cycling: A Southern Ocean perspective, *Geochem. Geophys. Geosyst.*, *9*, Q02006, doi:10.1029/2007GC001736.

Sosdian, S., and Y. Rosenthal (2009), Deep-sea temperature and ice volume changes across the Pliocene-Pleistocene climate transitions, *Science*, *325*(5938), 306–310, doi:10.1126/science.1169938.

Spero, H. J., J. Bijma, D. W. Lea, and B. E. Bemis (1997), Effect of seawater carbonate concentration on foraminiferal carbon and oxygen isotopes, *Nature*, *390*, 497–500, doi:10.1038/37333.

Spero, H. J., J. Bijma, D. W. Lea, and A. D. Russell (1999), Deconvolving glacial ocean carbonate chemistry from the planktonic foraminifera carbon isotope record, in *Reconstructing Ocean History: A Window Into the Future*, edited by F. Abrantis and A. Mix, pp. 329–342, Kluwer Acad., New York, doi:10013/epic.16652.

Stanley, S. M., and L. A. Hardie (1998), Secular oscillations in the carbonate mineralogy of reef-building and sediment-producing organisms driven by tectonically forced shifts in seawater chemistry, *Palaeogeogr. Palaeoclimatol. Palaeoecol.*, *144*(1–2), 3–19, doi:10.1016/S0031-0182(98)00109-6.

Stanley, S. M., J. B. Ries, and L. A. Hardie (2005), Seawater chemistry, coccolithophore population growth, and the origin of Cretaceous chalk, *Geology*, *33*(7), 593–596, doi:10.1130/G21405.1.

Toggweiler, J. R. (2008), Origin of the 100,000-yr time scale in Antarctic temperatures and atmospheric CO_2, *Paleoceanography*, *23*, PA2211, doi:10.1029/2006PA001405.

Toggweiler, J. R., and H. Bjornsson (2000), Drake Passage and palaeoclimate, *J. Quat. Sci.*, *15*(4), 319–328, doi:10.1002/1099-1417(200005)15:4<319::AID-JQS545>3.0.CO;2-C.

Toggweiler, J. R., and B. Samuels (1995), Effect of Drake Passage on the global thermohaline circulation, *Deep Sea Res., Part I*, *42*(4), 477–500, doi:10.1016/0967-0637(95)00012-U.

Tripati, A. K., M. L. Delaney, J. C. Zachos, L. D. Anderson, D. C. Kelly, and H. Elderfield (2003), Tropical sea-surface temperature reconstruction for the early Paleogene using Mg/Ca ratios of planktonic foraminifera, *Paleoceanography*, *18*(4), 1101, doi:10.1029/2003PA000937.

Tripati, A., J. Backman, H. Elderfield, and P. Ferretti (2005), Eocene bipolar glaciation associated with global carbon cycle changes, *Nature*, *436*(7049), 341–346, doi:10.1038/nature03874.

Van Andel, T. H. (1975), Mesozoic/Cenozoic calcite compensation depth and the global distribution of calcareous sediments, *Earth Planet. Sci. Lett.*, *26*(2), 187–194, doi:10.1016/0012-821X(75)90086-2.

Veizer, J., et al. (1999), $^{87}Sr/^{86}Sr$, $\delta^{13}C$ and $\delta^{18}O$ evolution of Phanerozoic seawater, *Chem. Geol.*, *161*(1–3), 59–88, doi:10.1016/S0009-2541(99)00081-9.

Waelbroeck, C., L. Labeyrie, E. Michel, J. C. Duplessy, J. F. McManus, K. Lambeck, E. Balbon, and M. Labracherie (2002), Sea-level and deep water temperature changes derived from benthic foraminifera isotopic records, *Quat. Sci. Rev.*, *21*(1–3), 295–305, doi:10.1016/S0277-3791(01)00101-9.

Walker, J. C. G., P. B. Hays, and J. F. Kasting (1981), A negative feedback mechanism for the long-term stabilization of Earth's surface temperature, *J. Geophys. Res.*, *86*(C10), 9776–9782, doi:10.1029/JC086iC10p09776.

Wallmann, K. (2001), The geological water cycle and the evolution of marine $\delta^{18}O$ values, *Geochim. Cosmochim. Acta*, *65*(15), 2469–2485, doi:10.1016/S0016-7037(01)00603-2.

Wallmann, K. (2004), Impact of atmospheric CO_2 and galactic cosmic radiation on Phanerozoic climate change and the marine $\delta^{18}O$ record, *Geochem. Geophys. Geosyst.*, *5*, Q06004, doi:10.1029/2003GC000683.

White, T., L. Gonzalez, G. Ludvigson, and C. Poulsen (2001), Middle Cretaceous greenhouse hydrologic cycle of North America, *Geology*, *29*(4), 363–366, doi:10.1130/0091-7613(2001)029<0363:MCGHCO>2.0.CO;2.

Wilkinson, B. H., and T. J. Algeo (1989), Sedimentary carbonate record of calcium-magnesium cycling, *Am. J. Sci.*, *289*(10), 1158–1194, doi:10.2475/ajs.289.10.1158.

Wilson, D. S., and B. P. Luyendyk (2009), West Antarctic paleotopography estimated at the Eocene–Oligocene climate transition, *Geophys. Res. Lett.*, *36*, L16302, doi:10.1029/2009GL039297.

Wilson, D. S., S. S. R. Jamieson, P. J. Barrett, G. Leitchenkov, K. Gohl, and R. D. Larter (2011), Antarctic topography at the Eocene–Oligocene boundary, *Palaeogeogr. Palaeoclimatol. Palaeoecol.*, doi:10.1016/j.palaeo.2011.05.028, in press.

Wright, J. D., and K. G. Miller (1996), Control of North Atlantic Deep Water circulation by the Greenland-Scotland Ridge, *Paleoceanography*, *11*(2), 157–170, doi:10.1029/95PA03696.

Yu, J., and H. Elderfield (2008), Mg/Ca in the benthic foraminifera Cibicidoides wuellerstorfi and Cibicidoides mundulus: Temperature versus carbonate ion saturation, *Earth Planet. Sci. Lett.*, *276*(1–2), 129–139, doi:10.1016/j.epsl.2008.09.015.

Zachos, J. C., J. R. Breza, and S. W. Wise Jr. (1992), Early Oligocene ice-sheet expansion on Antarctica: Stable isotope and sedimentological evidence from Kerguelen Plateau, southern Indian Ocean, *Geology*, *20*, 569–573, doi:10.1130/0091-7613(1992)020<0569:EOISEO>2.3.CO;2.

Zachos, J. C., M. Pagani, L. Sloan, E. Thomas, and K. Billups (2001), Trends, rhythms, and aberrations in global climate 65 Ma to Present, *Science*, *292*, 686–693, doi:10.1126/science.1059412.

Zachos, J. C., G. R. Dickens, and R. E. Zeebe (2008), An early Cenozoic perspective on greenhouse warming and carbon-cycle dynamics, *Nature*, *451*(7176), 279–283, doi:10.1038/nature06588.

Zeebe, R. E. (1999), An explanation of the effect of seawater carbonate concentration on foraminiferal oxygen isotopes, *Geochim. Cosmochim. Acta*, *63*(13–14), 2001–2007, doi:10.1016/S0016-7037(99)00091-5.

Zeebe, R. E. (2001), Seawater pH and isotopic paleotemperatures of Cretaceous oceans, *Palaeogeogr. Palaeoclimatol. Palaeoecol.*, *170*(1–2), 49–57, doi:10.1016/S0031-0182(01)00226-7.

P. J. Barrett, Antarctic Research Centre, Victoria University, Wellington 6001, New Zealand.

B. S. Cramer, Theiss Research, PO Box 127, La Jolla, CA 92038, USA. (b.s.cramer@theissresearch.org)

K. G. Miller and J. D. Wright, Department of Earth and Planetary Sciences, Rutgers, State University of New Jersey, Piscataway, NJ 08854, USA.